Demise of a harbor: A geochemical chronicle from Ephesus

Authors version of an article in JOURNAL OF ARCHAEOLOGICAL SCIENCE · OCTOBER 2014
DOI: 10.1016/j.jas.2014.10.002

Hugo Delile[1,2*], Janne Blichert-Toft[2,3], Jean-Philippe Goiran[4], Friederike Stock[5], Florent Arnaud-Godet[2], Jean-Paul Bravard[1], Helmut Brückner[5], Francis Albarède[2,3],

[1]*Université Lumière Lyon 2, CNRS UMR 5600, 69676 Bron, France*
[2]*Ecole Normale Supérieure de Lyon, Université Claude Bernard-Lyon 1, CNRS UMR 5276, 69364 Lyon Cedex 7, France*
[3]*Department of Earth Science, Rice University, Houston, TX 77005, USA*
[4]*Maison de l'Orient et de la Méditerranée, CNRS UMR 5133, 69365 Lyon Cedex 7, France*
[5]*Institute of Geography, University of Cologne, Albertus-Magnus-Platz, 50923 Cologne (Köln), Germany*

*Corresponding author: hdelile@gmail.comTel: +33 6 82 73 66 53

Abstract

At the end of the first century BC, Ephesus became the Roman capital of Asia Minor and the most important commercial, religious, and cultural center of the region. In order to evaluate the status of anthropogenic fluxes in the port of Ephesus, a 12 m long sediment core drilled in the Roman basin was investigated to shed light on the paleo-environmental evolution of the harbor using grain size distribution analysis, ^{14}C ages, major and trace element geochemistry, and Pb isotope compositions. With the help of complementary sedimentological data and Principal Component Analysis, five distinct units were identified which, together, reflect the different stages of water history in the harbor. Among the major disruptive events affecting the port were earthquakes and military events, both of which were particularly effective at destroying the water distribution system.

Seasonal floods of the Cayster River (Küçük Menderes) were the major source of the silt that progressively infilled the harbor. Silting in was further enhanced by the westward migration of the river mouth. A single major disruptive event located at 550 cm core depth and heralding the development of anoxia in the harbor marks the end of the dynamic regime that otherwise controlled the harbor water throughout the Roman Empire period. This remarkable *event may correspond to a major disruption of the aqueduct system or to a brutal avulsion of the Cayster River bed. It clearly represents a major disturbance in the history of life at Ephesus. It is poorly dated, but probably occurred during the reign of Augustus or shortly after. Lead isotope and trace metal evidence suggest that in the four bottom units pollution was subdued with respect to other Pb metal inputs, presumably those from aqueducts and natural karstic springs. Near the top of the core, which coincides with harbor abandonment and the more recent period, anthropogenic Pb contamination is clearly visible in both Pb abundances and isotopic compositions.*

Keywords: Harbor geoarcheology, geochemistry, Pb isotopes, Roman age, paleo-pollution, Ephesus, Küçük Menderes

1. Introduction

Lead isotope studies have opened up a new, though somewhat controversial, perspective on the development of the manufacturing status of ancient cultures over the past several millennia (Hong et al., 1994). Isolated artifacts alone do not suffice to assess the broad and long-lasting aspects of antique trade routes. Lead isotopes constitute a complementary tool in that they play a critical role wherever their compositions can be ascribed to anthropogenic influence in the form of lead and heavy metal pollution of sediments accumulated in harbors, which are highly efficient traps for clays and suspensions. Anthropogenic impact using Pb isotopes as a tracer has so far been documented for the ancient harbors of Alexandria (Véron et al., 2006; 2013; Stanley et al., 2007), Sidon (Le Roux et al., 2003), Marseilles (Le Roux et al., 2005), and Rome (Delile et al., 2014a).

Applying similar methods to the Roman harbor of Ephesus is appealing because of the status of the Ephesus city port during Roman times as an exceptionally influential commercial and religious center of the ancient Mediterranean world. Ephesus was a major town of Asia Minor and has a long history that began in the 10^{th} century BC.. Its position at short distances from both the Dardanelles and the populated city states of southern Greece gave Ephesus a strategic role in all the wars affecting Asia Minor and the Aegean Sea since the Persian wars of the classical period. Its importance remained prominent during Hellenistic and Roman times and during the entire history of the Byzantine Empire, and only declined as a result of the Turkish conquest. Because sediments gradually filled in the inlet of the Cayster River (Küçük Menderes), the harbor of Ephesus repeatedly moved down river over the centuries (Kraft et al., 2000; 2011).

Here we use samples from a 12 m long sediment core taken in the Roman port of Ephesus to investigate the paleo-environmental and hydraulic evolution of the harbor using grain size distribution analysis, ^{14}C ages, major and trace element geochemistry, and Pb isotope compositions. We focus in particular on the relative abundances of Pb and other chalcophile elements in the harbor sediments and discuss the respective status of the anthropogenic and natural metal fluxes and their origins as deduced from the Pb isotope record.

2. Historical background

Literature on the history of Ephesus is abundant because of the wealth of ruins left by its different inhabiting cultures and its role in the history of this part of the world first as a major religious center dedicated to Artemis and later as one of the leading churches of the Mediterranean world. For a detailed historical context of the present work, the reader is referred to the well-documented textbook by Foss (1979) and to Scherrer (1995). Here we provide only a brief overview.

Different sites were inhabited in the immediate vicinity of classical Ephesus since the Neolithic culture and during the Bronze Age. The historical city (close to the Artemision) was founded in the 10th century BC by Ionians and became part of the Ionian League. The classic site (at the base of the western side of the Panayırdağ) was occupied around 300 BC under Lysimachus, one of Alexander's generals, but quickly passed under Seleucid and then Ptolemaic rules. After the Battle of Magnesia in 190 BC, Ephesus came under the domination of Pergamon, and finally became part of the Roman Republic in 133 BC. After the Mithridatic wars (ending in 63 BC), Augustus made Ephesus the capital of Asia Minor. At that stage, the surface area of the city, enclosed by the walls of Lysimachus, is thought to have extended over more than 2 km^2 and its population to have reached 50,000 inhabitants.

The city and its temple were destroyed by the Goths in 262 AD. But Ephesus was rebuilt and enlarged by Constantine and soon recaptured most of the importance it had held since Hellenistic times. A burst of seismic activity between 358 and 365 AD repeatedly destroyed major cities around the Aegean (Guidoboni, 1994), including Ephesus. In the 7th century AD, several additional disasters struck Ephesus, notably the major earthquake of 614 AD, as well as the repeated sacks by Arab, Frankish, and Turkish raiders. Western Turkey is well known for being subjected to frequent earthquakes of large magnitude (e.g., Vannucci et al., 2004). Although some dates are not well established, particularly severe earthquakes persistently ravaged the city in AD 17, 23, 47, 178, 194, 262, 275, 337, 358 to 365, and 614 (Guidoboni, 1994; Foss, 1979). In AD 1304, what was by then left of Ephesus fell into the hands of the Turks, and its population was either deported or massacred. These adverse troubles combined with the final stages of insilting of the harbor basin, which had incessantly plagued harbor activity since its early Hellenistic days (Strabo, XIV.1.24), precipitated the demise of the harbor and the city it served.

3. The study area

Ephesus' harbor lies on the Aegean coast of Turkey at the western extremity of the Küçük Menderes graben (KMG) (Fig. 1). The KMG corresponds to the catchment area of the Küçük Menderes (Cayster) river, which is divided into five sub-basins delimited by pre-Miocene geology (Rojay et al., 2005). The surrounding hills are composed of crystalline marble or partially dolomitic breccias of Mesozoic age (Vetters 1989; Çakmakoğlu, 2007). The hills over which Ephesus aqueducts run also include Paleozoic crystalline rocks such as granites, gneisses, and micaschists. Water was brought to the city by up to seven aqueducts built between Archaic times and the Roman Empire and repaired during different periods, notably after major earthquakes. This point is particularly important since all the waters from the aqueducts terminated in the harbor where they were susceptible to mixing with Cayster river water, marine water, and waste waters of public (baths, fountains) and domestic usage, as well as with water from local workshops (Ortloff and Crouch, 2001).

The variation of relative sea level and the westward migration of the shoreline since Antiquity have been studied by Brückner (2005) and Pavlopoulos et al. (2012). Each century the shoreline progressed westward by, on average, ~350 m. Comparison of the apparent sea level changes with the values predicted by the regional model of Lambeck and Purcell (2005) indicates that subsidence of the coastline next to Ephesus since the classical period was of the order of 3 to 7 meters.

Georcheological research has been carried out at the Ephesus site and in the delta of the Cayster river since the 1990s (Brückner, 1997; 2005; Kraft et al., 1999; 2000; 2001; 2011; Stock et al., 2013; 2014). Besides reconstruction of the successive paleo-environments and the coastline as it has existed since 6000-–5000 BC (Fig. 1), this work also has shown that delta progradation led to multiple westward resettlements of the harbor. The ceaseless fight against silting to maintain the harbor of Ephesus as a functioning port during the Hellenistic period is first and foremost reflected in the displacement of the city to the western side of mount Pion (Panayırdağ) by Lysimachus in ~290 BC (Scherrer, 1995).

4. Analytical techniques

A sediment core about 12 m long (EPH 276) was drilled in the hexagonal Roman harbor basin of Ephesus (Fig. 1). We sampled the core at high resolution by taking a total of 111 samples (one sample every 10 cm). The samples were analyzed for grain size distributions (see Stock et al., 2013, for details), major and trace element concentrations (Table S1; see Delile et al., 2014b, for details), and Pb isotope compositions (Table S2; see here below and Delile et al., 2014a, for details). Lead isotope compositions were obtained not on the bulk sediment, but, in order to isolate potential anthropogenic components, on HBr leachates. The leaching procedure consisted in first treating the samples with chloroform to remove most of the organic fraction, then, after rinsing the residues with clean water, leaching them with dilute HBr including ultrasonicating and heating steps. As shown for Portus (Delile et al., 2014a), this technique enhances the contrast between Pb held in surface contamination-prone coatings and detrital silicates. Carbonates also dissolve during the leaching process, but Pb contents of detrital carbonates are naturally low. As for carbonates precipitated within the harbor, they are of biogenic origin (cf. discussion of series D and E below) likely meaning that isotope information obtained on carbonate-rich samples is consistent with that derived from the leachates of the rest of the sample series. The HBr leach fraction was recovered for Pb separation by anion-exchange chromatography using HBr as eluent of the sample matrix and HCl as eluent of the Pb. Lead was also separated from the residues of 16 of the 111 EPH 276 samples. The amounts of Pb extracted from all samples were large (>1 µg) and orders of magnitude above the total procedural blank of ~20 pg. The purified Pb was analyzed for its isotopic composition by multiple-collector inductively coupled plasma mass spectrometry (Nu Plasma 500 HR) at ENS

Lyon using Tl for instrumental mass bias correction and bracketing the samples with the NIST 981 standard for which the values of Eisele et al. (2003) were used.

Six samples were AMS-^{14}C-dated (Table S3), complementing the chronostratigraphy of neighboring cores analyzed by Stock et al. (submitted). The Carbon-14 ages were obtained on fragments of wood, vegetal matter, seeds, and pollen, and are listed in Table S3 and shown in Figs. 2 and 3. Errors on raw radiocarbon ages BP are reported at the 95 percent confidence level (two sigma). The measured ^{14}C (BP) ages were converted into BC – AD dates relative to the continental and marine curves of Reimer et al. (2009) using the Clam software (Blaauw, 2010).

Interpretation of the analytical results rests on different methods of data processing. We applied Principal Component Analysis (PCA) and Factor Analysis to major and trace element concentration data, as well as loss-on-ignition (L.O.I.) (Fig. 2). In the very large data sets typical of those that modern geochemistry can now produce, observations are often correlated. A common case is that of the dilution of elements in sediments by detrital quartz. Such effects render the reading of the underlying causes of geochemical variation and their number difficult. PCA consists in rotating the data in their multidimensional space to convert them into uncorrelated variables known as principal components. Uncorrelated does not equate with independent, however, implying that small changes in rotation may affect all the principal components. PCA generally demonstrates that the variability of the observations can be accounted for by a very small (2-4) subset of variables that carry the bulk of the total variance. Principal components can be calculated from the covariance matrix or from the correlation matrix. Factor Analysis is a related technique that searches for the minimum variance for an arbitrary number of uncorrelated variables. It usually starts with PCA and implements different modes of rotation and weighing.

In addition to the PCA and Factor Analysis we also converted the Pb isotope compositions into their corresponding geochemically informed parameters, which are the model age T_{mod} and the $^{238}U/^{204}Pb$ (μ) and Th/U (κ) ratios (Table S2) using the equations given by Albarède et al. (2012), who also justified the advantages of this representation over those based on raw Pb isotope ratios. In short, T_{mod} is a proxy for the tectonic age of crystalline rocks and their associated ore deposits (or depositional age for sediments), while μ is the $^{238}U/^{204}Pb$ and κ the Th/U ratio of the province in which these rocks formed. T_{mod} closely maps the distribution of the Alpine, Hercynian, and early Paleozoic provinces of Europe, while μ delineates collision belts, and κ is a geochemical parameter with a remarkable regional consistency related to uplift and erosion. Maps of these parameters can be used to divide Europe into coherent regions (Delile et al., 2014a), which justify the use of T_{mod}, μ, and κ to determine provenance of archeological artifacts. T_{mod}, μ, and κ in turn provide a rapid characterization of the geological environment in which ores formed. A Matlab code is given in Appendix A and an Excel spreadsheet in which to calculate these parameters will be provided upon request. As mentioned above, T_{mod} represents the tectonic age of the geological province to which a given sample belongs, while μ is best perceived as an indicator of whether this province is a collision range or a tectonically stable area. The variable κ distinguishes upper crust with low κ values from middle and lower crust with higher κ values (Albarède et al., 2012). The precision and accuracy of T_{mod} is typically of a few tens of Ma, but, occasionally, the T_{mod}-μ-κ model fails when the underlying closed-system assumption breaks down due to U addition by recent weathering or hydrothermal activity.

5. Sedimentary units and the age-depth model

The core has been divided into five different units labeled A, B, C, D, and E on the basis of the sedimentological and geochemical traits described in Fig. 3A; they span the entire period of activity of the Hellenistic, Roman, and Byzantine harbor (Table 1).

Unit A (1200-1080 cm) exhibits alternating brown and grey varves composed of massive clayey silts with the presence of several beige to ocher fine layers. The C/M plot (Fig. 3B) indicates that the depositional processes are represented by mixed decantation and graded suspension. Units B and C (1080-515 cm) are characterized by grey to greenish massive sandy silts with the presence of several beige to ocher fine layers enriched in sand. This deposit was deposited as a graded suspension with embedded fine layers derived from mixed processes of graded and uniform suspension. Unit D (515-290 cm) consists of dark to greyish silts with variable clay (bottom) and sand (top) enrichments. From bottom to top, deposit processes evolve from mixed uniform and graded suspension to a blend with graded and uniform suspensions. Unit E (< 290 cm) is composed of beige sandy silts with phragmite vegetal remains. The depositional processes point mostly to mixed graded and uniform suspensions.

The age-depth model is based on six ^{14}C ages (Fig. 4, Table S3). The four oldest ^{14}C ages fall within a narrow time interval and are statistically indistinguishable. An approximate seven meters of sediment were deposited in a few tens of years during the reign of Augustus or shortly after. Such an extraordinarily fast sedimentation rate is consistent with a periodogram analysis (e.g., Albarède, 1995) of the magnetic susceptibility record. The periodogram, which is the equivalent of a Fourier transform for unequally spaced data, identifies prominent periodic fluctuations in the targeted property, here the magnetic susceptibility. After removal of long-term variations (de-trending) by fitting a fourth-degree polynomial, the shortest values with significance level $P > 0.95$ occur at 20 and 24 cm (Fig. 5). Longer wavelength peaks probably reflect climatic effects or are artifacts of de-trending. Assuming a seasonal cause for the observed susceptibility fluctuations therefore indicates a sedimentation rate of ~20 cm per year, equivalent, over the 7 meters of sediment with the oldest ^{14}C ages, to ~35 years of sedimentary history. In contrast, the average sedimentation rate between the top three ^{14}C samples (early and late Byzantine) is only ~0.2 cm a^{-1}.

6. Results and discussion

6.1. Harbor hydraulics

In order to understand the hydraulic dynamics of the harbor, we first need to estimate its water capacity. The approximate dimensions taken from aerial photographs lead to a volume of (500 × 400 ×5) m^3 = 1.0 × 10^6 m^3 (see also Kirbihler, 2013; Stock et al., submitted). We assume that most of the sedimentary layers were deposited during short seasonal flood events of the Cayster River, whereas water running into the harbor came from different potential sources: seawater, runoff, karstic springs, and aqueducts. Seawater and water from springs and aqueducts must have been largely clear of sedimentary particles. Karstic springs are common in the area around the modern Lake Kocagöz (Somay et al., 2008; Somay and Gemici, 2009), which today exists on the site of the ancient harbor basin. A seawater component is present in the water from all the lakes, including Lake Kocagöz (Somay et al., 2008; Somay and Gemici, 2009). Such a component attests to a contribution from spring waters contaminated by marine intrusions into the karst. As for other water inputs, Kraft et al. (2007) pointed out that all the city sewage was diverted into the Great Harbor.

The up to seven aqueducts built during the existence of the Ephesus port carried substantial volumes of water into the harbor. Wiplinger (2013) quotes an estimate of 0.6 m^3 s^{-1} for the Derğirmendere aqueduct alone. Using the model by Ortloff and Crouch (2001), we surmise that the total water distribution to the city from the fully-functional aqueducts at the peak of city prosperity may have been over ~2 m^3 s^{-1}. This number is substantial with respect to the mean discharge of ~11.45 m^3 s^{-1} inferred for the river, not including flood events (Vliegenthart et al., 2007), indicating that if other inputs such as karstic springs and runoff are disregarded, water in the harbor was replaced by the aqueducts in merely six days. This estimate is of course an average estimate and during seasonal droughts the ingress of seawater attested to by the presence of brackish fauna also contributed to the harbor's overall water budget.

Water output is difficult to constrain independently. The harbor canal, whose construction may have started as early as during the first century AD when the shoreline swept past the harbor, was narrow at the harbor entrance (Kraft et al., 2007). Assuming a cross-section at the narrowest point of ~50 m^2 would imply that aqueduct-delivered water was leaving the canal at a rate of 145 m per hour, probably fast enough to limit water ingress from the sea under fair weather conditions. This velocity must have been reduced by the effect of draught and evaporation during the dry (hot) season, and increased by local springs during the wet (cold) season. The presence of brackish water ostracods and occasional occurrence of marine foraminifera (Stock et al., submitted) demonstrate that the flow could occasionally be reversed, presumably as a result of a low water table and reduced precipitation during the dry season. Over time, the harbor was nevertheless affected by westward delta progradation and proximity to the mouth of the Cayster river (Fig. 1): by the end of the 2nd century BC, the delta had advanced as far as the Great Harbor (Kraft et al., 2007) and the canal had to be extended, thus limiting ingress of seawater into the harbor basin even further.

To summarize harbor hydrodynamics, the 'normal' situation is that of a basin steadily filled by polluted urban water initially brought to the harbor by aqueducts and local springs and quickly evacuated through a canal with little ingress from the sea. As long as the coastline is not too distant, some seawater may be admitted during the dry season, while floods of, in the present case, the Cayster River dominated the water balance during spells of heavy rain. Silting in of the harbor would have been caused only by floods, which today are known to carry up to 100–150 $m^3\ s^{-1}$of water (Vliegenthart et al., 2007). The Romans went to great length to protect the harbor from river floods. Kraft et al. (2000; 2011) mention that, in the early 2nd century AD, Hadrian sought to divert the Cayster River with an 18 m high dam and also made multiple attempts to dredge the harbor.

6.2. Environmental conditions in the harbor basin

In order to assess the environmental conditions that prevailed during sedimentation, we plotted the concentrations of first-row transition elements (Ti-Zn) and other metallic elements (Ga, Pb, Mo, Bi, Cd, Ag, As, and Sb) normalized to the upper-crust concentrations of Rudnick and Gao (2003) (Fig. S1). Factor analysis of major and trace element abundances leads to the identification of three major components.

1. *The first factor* opposes elements indicative of the detrital load of the river (Al, Ti, Mg, etc.) to those distinctive of carbonate minerals (Ca, Sr) and L.O.I.
2. *The second factor* singles out chalcophile elements that, as attested to by the presence of sulfur in this group, precipitate as sulfide under anoxic conditions (Pb, Ag, Cu, Ni, Mo), or are particularly sensitive to redox conditions (U, Cr). When the elements embedded in this factor are normalized to Al (Fig. 6), as a means of accounting for the variable abundance of the detrital component, and plotted against depth in the core, a sharp increase is observed at 520 cm depth. The significance of this factor deserves some discussion because Pb, Ag, and Cu may also be seen as representing an anthropogenic component. Figures 6 and S1 further show the striking consistency of these metals among themselves and with respect to sulfur. Such regular behavior is not supportive of random contamination by a particular metal, such as Pb. The Mo-Pb correlation is very strong (r=0.90 excluding the top five samples likely contaminated by gasoline Pb) as is the Ag-Pb correlation (r=0.95). This factor therefore reflects more on changing redox conditions in the harbor than on anthropogenic pollution.

3. *The third factor* is dominated by La, Ce and, to a lesser extent, Se. Most other loadings are very small, except possibly P. The weak negative correlation between excess La and Ce on the one hand and P deficit on the other hand suggests the presence of non-phosphatic rare-earth minerals, such as allanite, notably in the coarse silts between 515 an 650 cm.

The accumulation of so much sediment in a matter of decades requires an explanation, especially since the thickness of the newly deposited layers exceeds the water depth usually assumed for the harbor (4–6 m), even next to the mole (Stock et al., submitted). One factor clearly is the westward progradation of the shoreline past the harbor at about the time of fast sedimentation. F. Stock (personal communication) obtained a ^{14}C age of 44 BC – AD 52 for the silting in of the harbor canal consistent with the present finding. The sharp geochemical discontinuities at 650 and 550 m are flagged by strong peaks of magnetic susceptibility (Fig. 3A). The efficiency of sediment confinement by the harbor prior to the three lowermost units is staggering, while the sudden drop in sedimentation rate and the short but intense episodes of high magnetic susceptibility require the intervention of a brutal event. A probable cause for this discontinuity is an abrupt jump of the Cayster River channel triggered by the abandonment of a meander (avulsions) or by exceptional floods (Brown, 1997). Co-seismic vertical movements (Pavlopoulos et al., 2012) associated with the major AD 17, 23, and 47 earthquakes may also have played a role.

The lowermost *unit A* (1200–1080 cm) was deposited during the Roman Republic. It is consistently dominated by silt (F1>0) with anoxic influence (F2<0). The anoxic conditions of the basin bottom as attested to by abundant S, Mo, and U (Fig. 2), small excesses of Mo and Ag (Fig. S1), and persistence of seasonal varves, indicate that the terrigenous flux into the early Roman harbor of Ephesus during the 1st century BC was not noticeably oxidized whether water input was freshwater or seawater. Grain size distribution (Fig. 3) reflects an environment where decantation is important (Bravard and Peiry, 1999; Bravard et al., 2014). Input of oxygenated freshwater into the harbor, regardless of its source, therefore was limited and whatever water was added by the aqueduct system must have been dominated by sewage.

Unit B (1080–650 cm) continues to show the prevalence of the detrital flux (F1 >0), but now with evidence of oxygenation (F2 ≥0). The transition-element pattern typically is crustal in origin and no visible anomaly of Mo and Ag is observed (Fig. S1). Grain-size analysis indicates graded grain size distributions by turbulent waters, reflecting that, even at times of flood, water was being constantly evacuated from the harbor. Ephesus counted up to seven aqueducts implying that the early Roman harbor was saved from silting in as much by water from its many aqueducts continuously flushing the basin as by the Roman engineers. As shown by the return of some decantation events (Fig. 3), the aqueducts made silting depend on a fully functioning water distribution system. In this respect, the Menderes area is seismically active (Vannucci et al., 2004) and major earthquakes were particularly disruptive to the long and complex Ephesus aqueduct network (Passchier et al., 2013). Reduction of the water input by the seismic destruction of aqueducts translates into reduced water egress from the harbor basin and hence enhanced efficiency of its role as a sediment trap. Silting in of the harbor in the aftermath of major earthquakes therefore became collateral damage to the rest of the disasters caused by the seismic activity.

Transition to *unit C* (Fig. 2) (650–550 cm) is heralded by a peak of magnetic susceptibility (Fig. 3A). Highly negative values of factor 3, i.e., higher Se, La, and Ce contents, reflect lesser dilution of minor elements by quartz and carbonate. The variation patterns of transition elements and other metals are very similar to those of unit B. As already observed for rivers (Yang et al., 2002), a strong correlation exists between grain size and lanthanide concentrations (Zhang et al., 1998; Yang et al., 2002). This geochemical change is consistent with a sand fraction in unit C smaller than that in unit B. Unit C shows some transient geochemical features

(Fig. 7), true harbingers of the major changes that would profoundly affect unit D, notably an increase in sulfur and heavy metal contents

The transition (550-515 cm) between unit C and *unit D* (515-300 cm) also is announced by a strong peak of magnetic susceptibility (Fig. 3A), corresponding to a strong compositional shift with a surge of the biogenic component (F1<0) due to degraded ventilation of bottom waters by eutrophication (F2<0). Sulfide reduction and precipitation is attested to by a sudden two-order-of-magnitude increase in the S/Al ratio (Fig. 6). The surge in sulfur, Zn, Ni, and Co conspicuously follows the surge of Ca, Pb, Ag, Cu, Cd, Mo, and Cr by some 30 cm in the core. This delay, which may have been as short as a few years and possibly was only one or two years, is visible in the plot of Fig. 7 as a pronounced negative excursion of ratios such as Ca/S, Mo/S, and Pb/S between 520 and 550 cm depth. These characteristics together with high Sr abundance and the presence of fine calcareous layers (Kylander et al., 2011; Martín-Puertas et al., 2011) show that sulfide precipitation predated the development of eutrophic conditions manifested by the rise in Ca and was due to the sudden isolation of the harbor from ventilated waters. The trend of decreasing ratios of chalcophile elements relative to sulfur, which was perceptible already in the early harbor, markedly changes at the C-D boundary, and the rate at which these ratios change significantly increases as well. Again, the correlation between Cr, Cu, Pb, Mo, and Ag (Figs. 6, 7, S1) excesses are not in favor of selective pollution by metallurgical or any other industrial activities. The destruction of the aqueducts by the major earthquakes ravaging the city, such as the AD 17, 23, and 47 events (see a discussion in Guidoboni, 1994), and the AD 64 AD cleaning credited to Barea Soranus by Tacitus (XVI,23) may have combined with the increasing silting of the harbor entrance upon westward progradation of the delta (Fig. 1) (Brückner, 2005) to modify the hydraulic regime of the harbor. The top of unit D records a short-lived return of better oxygenated conditions which, with the caution due the age-depth model, may correspond to the revival of the harbor by Justinian (early and mid- 6th century; Foss, 1979; Scherrer, 1995).

The age-depth model (Fig. 4) places the transition between units D and E (~300 cm) in the 9th century. Carbonate precipitation dominates unit E as it did the lower part of unit D (F1<0) indicating a negative water balance (Fig. 2B; Martín-Puertas et al., 2011; Delile et al., 2014b). Excesses of Cr, Cu, Mo, and Ag are still well correlated (Fig. 2A) and confirm the persistence of a sulfur-rich, oxygen-deficient eutrophic regime, but, as shown by the positive F2 values, with oxygen deficiency being less pronounced than in the underlying unit D. The water deficit caused conditions to evolve towards a peatland environment consistent with the considerable extension of the Cayster delta at this time (Fig. 1). The modern estuary of the Küçük Menderes is wetland dotted with alkaline lakes recharged from precipitation and local karstic springs. In late Byzantine times, the harbor may have been functional, but appears to have been increasingly cut off from the sea and the river (Kraft et al., 2011) (Fig. 1). Some of the shallow core samples show excess Pb of probable but uncertain anthropic origin (Fig. 8).

To sum up on environmental conditions, core EPH-276 holds the record of anoxic conditions prevailing at times in the harbor, likely compromising the control of harbor hydrodynamics by human activities. Lead isotopes are expected to shed light on the magnitude of anthropogenic contamination at the time of sediment deposition and this is what the next section will be addressing.

6.3. Interpretation of Pb abundance and isotopic signals

Here we focus on the Pb isotope compositions of the leached fractions only because this is where chances of observing anthropogenic input are maximum. Figure 8 shows the Pb/Al ratio together with the Pb isotope data in the form of three geochemical parameters, T_{mod} (Ma = million years), μ, and κ. Based on these parameters and the enrichment factor of Pb as represented by Pb/Al and closely tracking F2, the chronostratigraphic evolution of these four curves shows remarkable discontinuities (Fig. 2). In agreement with what was discussed above for other metals, the transition between units A and B stands out clearly by a marked drop in Pb/Al. A subtle increase in μ and κ, while T_{mod} remains young (~80 Ma or Upper Cretaceous), is evidence of change in the sources of Pb. The next discontinuity takes place between units C and D. The increase in Pb/Al and Ca/Al is associated with older T_{mod} (~120 Ma or Early Cretaceous) and lower values of μ and κ. The Pb/Al ratio decreases steadily throughout unit D regardless of the changes in the major Ca/Al dip at 3.8 m depth that we assigned above to the 6th century. From unit D to E, most T_{mod} values exceed 240 Ma and the κ values decrease below the level of previous values. The samples at the top of the core seem to be largely influenced by a modern anthropogenic component.

The hydraulics of the harbor, notably its volume and output, may affect harbor oxygenation and thereby the metal contents of sediments. In contrast, changing Pb isotope compositions require changes in the relative contribution of all the sources of this metal. Lead isotopes reveal the nature and relative strengths of the following potential sources:

1. *Local natural sources*, which are multiple. Lead from the Cayster River comes during short-lived seasonal flood events. Seawater should be extremely poor in Pb, while brackish water from the estuary should be Pb-depleted by iron flocculation in the mixing zone. A contribution from the runoff and from karstic springs that discharge from marble-schists and marble-alluvium contacts (Somay et al 2008; Somay and Gemici 2009) should also be considered.
2. *Lead from the main water distribution system*. Such a component may come from the underground of the springs. It can also be acquired during transit from the aqueduct masonry, which includes mortar produced from local limestones. The laminated deposits observed in some aqueducts (Passchier et al., 2011; 2013) indicate hard water

with excess alkalinity, which does not favor the idea that Pb was leached out of these conduits. The seemingly high concentrations of chalcophile elements in the sediments, first and foremost Pb but also Co and Mo, do not entail a pollution signal.

3. *The network of aqueducts*, which is unlikely to be a major Pb contributor. The secondary water distribution system at Ephesus is dominated by *terra cotta* pipes and only rarely involves small-diameter lead pipes or fistulae (Ortloff and Crouch, 2001).

4. *Anthropogenic Pb* from local workshops or ballast dropped by merchant ships. Zabehlicky (1995) writes that a lead anchor 14.2 cm long was found during excavations, as well as lead interpreted as ballast, which as much as hinting at a potential source of pollution, signals that the dissolution of Pb artifacts is an exceedingly slow process. The presence of an arsenal on the harbor site at the time of Augustus was noted by Strabo (XIV.1.24). There is no doubt that a city with the population of Ephesus at its best periods would have to rely on local metallurgy. In sediments, however, a geochemical signal of pollution is difficult to detect, and to which extent Pb artifacts attest to wholesale contamination of harbor sediments is not clear. The stability of Pb isotope compositions over long periods of time (decades, even centuries) does not bring to mind metal supply in troubled times. Even more conclusive is the observation that, except for unit E, Cr, Cu, Mo, Ag, and Cu coherently track Pb and Ca: although these elements are sensitive to redox conditions, they were not involved in Pb metallurgy. The Pb/Ag ratio remains remarkably stable, while the record of Ni and Co, for which extractive metallurgy was unknown at the time and which additionally are not found in the same ores as Pb, also follow the Pb record with depth. The lesser impact of anthropogenic Pb pollution at Ephesus relative to Portus (Delile et al., 2014a) directly reflects that the urban water distribution systems used

different materials, *terra cotta* for the former (Ortloff and Crouch, 2001) and lead fistulæ for the latter.

The Cretaceous model ages of 80 Ma and 120 Ma observed in the lower part of the core are consistent with those of the carbonate hills surrounding Ephesus and may simply register Pb from the water distribution system (natural springs or conduits). This interpretation is supported by the similar Pb isotope compositions of leachate-residue pairs (Table S2). The residues of the samples with T_{mod} values >200 Ma have not been analyzed, but these ages are consistent with the age of the Paleozoic and Triassic crystalline basement of the Menderes Massif (Vetters, 1989; Bozkurt, 2007; Çakmakoğlu, 2007; Gürer et al., 2009) (see maps in the supplementary material of Delile et al., 2014a).

The appearance of old T_{mod} values shortly after the beginning of unit E, which have not been observed at earlier times, coincides with the onset of carbonate sedimentation (up to 45 wt.% CaO). Runoff and karstic springs more or less contaminated by seawater (Somay et al 2008; Somay and Gemici 2009) are therefore left as the main steady sources of water in the ancient port, which since has become the modern Lake Kocagöz. Two competing interpretations are left: (1) while ancient aqueducts were bringing in Cretaceous Pb, runoff and karstic springs now bring in Paleozoic Pb; or (2) old T_{mod} values reflect some anthropic influence of poorly constrained origin. The younger samples with T_{mod} values >200 Ma may represent sources in the Menderes region, but Pb from Thrace, or even from western Europe, cannot be excluded.

Historical evidence in favor of Ephesus hosting significant industrial activity in the 11th and 12th centuries (Foss, 1979, pp. 120-123), however, is faint. Foss (1979, p. 113) further argues that from the 8th century onwards the harbor district was literally abandoned. The center of town moved to the hill of Ayasuluk, while new ports, such as Scalanova (ancient Phygela) built on the site of modern Kuşadası, gradually took over the silted in harbor of Ephesus.

Nevertheless, from the middle of the 9th to the 10th century, the victories of the Byzantines against the Arabs in Asia Minor enabled Ephesus to regain a preeminent position in the Empire (Foss, 1979). A phase of economic development would be consistent with the influx of Hercynian Pb into the most recent harbor deposits. The 10th century medieval economic revolution in Europe favored the development of trade between Europe and the Orient. West or north European sources of Pb cannot be excluded for that period.

7. Concluding remarks

Major changes in the lithology, grain-size distribution, major and trace element chemistry, and Pb isotope compositions of the harbor sediments at Ephesus reflect the history of the water distribution system of this port, notably in response to the increasing and declining needs of a population inhabiting a city that at several points in history was one of the largest of the Eastern Mediterranean. Throughout its history, the Ephesus port was affected by major disruptive events in the form of earthquakes and invasions, both of which were particularly effective at destroying aqueducts.

Progressive silting in of the harbor responded to the westward migration of the coastline and to human maintenance aimed at keeping the harbor functional. A single major disruptive event located at 550 cm core depth and heralding a two-order-of-magnitude drop in sedimentation rate and the development of anoxia in the harbor is clearly visible in the major and trace element record. Although this event may have unidentified military or seismic causes, we favor a durable displacement of the river course, which starved the harbor from further silt input. Overall, despite the presence of metallic artifacts in the harbor, the record of metal concentrations, in particular the Pb isotope record, suggests that pollution of the harbor was subdued relative to other inputs, notably those of aqueducts, except near the time of harbor abandonment (unit E).

Dating and identifying the seemingly key event located in the present sediment core at 550 cm depth, as well as in other cores from the same basin, is a new and major challenge. This event conspicuously marks the end of the dynamic regime controlling the harbor water during all of the Roman Empire and clearly represents a major disturbance in the history of life in Ephesus.

Acknowledgements

We thank the Austrian Archaeological Institute (ÖAI, Wien), especially its director Sabine Ladstätter, for the possibility to work in Ephesus. The Turkish authorities kindly granted the research permits. The Young Scientist Program of the Agence Nationale de la Recherche (CNRS) and the Roman Mediterranean Ports program (ERC) provided financial and logistic support. We also acknowledge support of the ARTEMIS program for carrying out the SMA radiocarbon dating. We further thank the Institut National des Sciences de l’Univers for supporting the analytical facility at ENS Lyon. A. Wilson kindly provided his personal Mediterranean shipwreck database. Melis Somay gave advice on the karstic sources around Ephesus. Two generous and insightful, yet anonymous, reviews helped improve the manuscript.

Appendix A: Matlab code for T_{mod}, μ, and κ calculations

The input data should be provided as an Excel file input.xlsx made of three columns,holding $^{206}Pb/^{204}Pb$, $^{207}Pb/^{204}Pb$, and $^{208}Pb/^{204}Pb$.

```
% Matlab code for model age calculations (Francis Albarede)
%
A=xlsread('input.xlsx',1);
m=size(A,1); % find m the number of samples
% decay constants
l8=0.155125;l5=0.98485;l2=0.049475;
% common Pb parameters from Albarede and Juteau (1984)
xstar=18.7500;ystar=15.63;zstar=38.83; kappastar=3.90;mustar=9.66;
% Initialize
FF=zeros(m,1);mu=zeros(m,1);dmu=zeros(m,1);kappa=zeros(m,1);dkappa=zeros(m,1);Tmod=zeros(m,1);Tinit=
1;
```

```
T0=3.8; % Beginning stage 2 (Ga), see Stacey and Kramers (1975)
options=optimset('Display','off');
for i=1:m % loop through all samples
   x=A(i,1); y=A(i,2); z=A(i,3);
   myf=@(T)TmPb(T,T0,x,y);
   [Tmod(i),FF(i),exitflag(i,1)]=fsolve(myf,Tinit,options); % use Matlab fsolve with function TmPb
   T1=Tmod(i);
   dmu(i)=(x-xstar+mustar*(exp(l8*T1)-1))/(exp(l8*T0)-exp(l8*T1));
   mu(i)=mustar+dmu(i);
   dkappa(i)=(z-zstar+mustar*kappastar*(exp(l2*T1)-1)-kappastar*dmu(i)*(exp(l2*T0)-
exp(l2*T1)))/(exp(l2*T0)-exp(l2*T1))/mu(i);
   kappa(i)=kappastar+dkappa(i);
end
B=[A,1000*Tmod,mu,kappa,FF,exitflag]
% B holds columnwise the original ratios (A), the model age (in Ma), mu, kappa, the
% exit value of the function to solve (should be less than 1e-9) and an
% exit parameter (1 expected)

function F = TmPb(T,T0,x,y)
      mustar=9.66;
      xstar=18.7500;ystar=15.63; %AJ
      l8=0.155125;l5=0.98485;
      p0=(exp(l5*T0)-exp(l5*T))/(exp(l8*T0)-exp(l8*T))/137.8;
      p1=(exp(l5*T)-1)/(exp(l8*T)-1)/137.8;
      %
      if x~=xstar % Eq. 12 in Albarede et al. (2012)
         F=(y-ystar)/(x-xstar)-p0-mustar*(exp(l8*T)-1)*(p0-p1)/(x-xstar);
      else
         F=(y-ystar)-mustar*(exp(l8*T)-1)*(p0-p1);
      end
   end
```

References

Albarède F., 1995.*Introduction to Geochemical Modeling*. Cambridge University Press, Cambridge. pp. 543.

Albarède, F., Desaulty, A.-M., Blichert-Toft, J., 2012. A geological perspective on the use of Pb isotopes in Archaeometry. Archaeometry 54, 853–867.

Blaauw, M., 2010. Methods and code for “classical” age-modelling of radiocarbon sequences. Quaternary Geochronology 5, 512–518.

Bozkurt, E., 2007. Extensional v. contractional origin for the southern Menderes shear zone, SW Turkey: tectonic and metamorphic implications. Geological Magazine 144, 191–210.

Bravard, J.-P., Peiry, J.-L., 1999. The CM pattern as a tool for the classification of alluvial suites and floodplains along the river continuum, in: Floodplains: Interdisciplinary Approaches, Geological Society Special Publication. Marrott S.B. and Alexander J., London, pp. 259–268.

Bravard, J.-P., Goichot, M., Tronchère, H., 2014. An assessment of sediment-transport processes in the Lower Mekong River based on deposit grain sizes, the CM technique and flow-energy data. Geomorphology 207, 174–189.

Brown A. G., 1997.Alluvial geoarchaeology: floodplain archaeology and environmental change. Cambridge University Press, pp. 377.

Brückner, H., 1997. Geoarchäologische Forschungen in derWesttürkei: das Beispiel Ephesus. Passauer Schriften zur Geographie 15, 39–51.

Brückner, H., 2005. Holocene shoreline displacements and their consequences for human societies: the example of Ephesus in western Turkey. Zeitschrift für Geomorphologie 137, 11–22.

Çakmakoğlu, A., 2007. Pre – neogene tectonostratigraphy of Dilek Peninsula and the area surrounding Söke and Selçuk. Bulletin of the Mineral Research and Exploration 135, 1–17.

Delile, H., Blichert-Toft, J., Goiran, J.-P., Keay, S., Albarède, F., 2014a. Lead in ancient Rome's city waters. PNAS 111.

Delile, H., Mazzini, I., Blichert-Toft, J., Goiran, J.-P., Arnaud-Godet, F., Salomon, F., Albarède, F., 2014b. Geochemical investigation of a sediment core from the Trajan basin at Portus, the harbor of ancient Rome. Quaternary Science Reviews 87, 34–45.

Eisele, J., Abouchami, W., Galer, S.J.G., Hofmann, A.W., 2003. The 320 kyr Pb isotope evolution of Mauna Kea lavas recorded in the HSDP-2 drill core. Geochem. Geophys. Geosyst. 4, 8710.

Foss, C., 1979. Ephesus after antiquity: a late antique, byzantine and turkish city. Cambridge university press.

Guidoboni, E., 1994. Catalogue of ancient earthquakes in the Mediterranean area up to the 10th century. Istituto nazionale di geofisica, Rome, Italie.

Gürer, Ö.F., Sarica-Filoreau, N., Özburan, M., Sangu, E., Doğan, B., 2009. Progressive development of the Büyük Menderes Graben based on new data, western Turkey. Geological Magazine 146, 652–673.

Hong, S., Candelone, J.-P., Patterson, C.C., Boutron, C.F., 1994. Greenland Ice Evidence of Hemispheric Lead Pollution Two Millennia Ago by Greek and Roman Civilizations. Science 265, 1841–1843.

Kirbihler, F., 2013. Les nauclères, l'entretien du port et l'implication des gens de mer dans la vie civique éphésienne, in: Gens De Mer: Ports Et Cités Aux Époques Ancienne, Médiévale Et Moderne, Histoire. Rennes : Presses universitaires de Rennes, pp. 111–126.

Kraft, J.C., Brückner, H., Kayan, İ., 1999. Palaeogeographies of Ancient Coastal Environments in the Environs of the Feigengarten Excavation and the "Via(e) Sacra(e)" to the Artemision at Ephesus, in: Steine und Wege. Festschrift für Dieter Knibbe zum 65. Geburtstag, Sonderschriften. P. Scherrer et al., Österreichisches Archäologisches Institut, pp. 91–100.

Kraft, J.C., Kayan, I., Brückner, H., 2001. The geological and paleogeographical environs of the Artemision, in: Der Kosmos Der Artemis Von Ephesos, Sonderschriften,. U. Muss, Österreichisches Archäologisches Institut, Vienna, pp. 123–133.

Kraft, J.C., Kayan, I., Brückner, H., Rapp, G., 2000. A Geological Analysis of Ancient Landscapes and the Harbors of Ephesus and the Artemision in Anatolia, in: Jahreshefte Des Österreichischen Archäologischen Institutes in Wien. pp. 175–233.

Kraft, J.C., Brückner, H., Kayan, İ., Engelmann, H., 2007. The geographies of ancient Ephesus and the Artemision in Anatolia. Geoarchaeology 22, 121–149.

Kraft, J.C., Rapp, G., Brükner, H., Kayan, İ., 2011. Results of the struggle at ancient Ephesus: natural processes 1, human intervention 0. Geological Society, London, Special Publications 352, 27–36.

Kylander, M.E., Ampel, L., Wohlfarth, B., Veres, D., 2011. High-resolution X-ray fluorescence core scanning analysis of Les Echets (France) sedimentary sequence: new insights from chemical proxies. Journal of Quaternary Science 26, 109–117.

Lambeck, K., Purcell, A., 2005. Sea-level change in the Mediterranean Sea since the LGM: model predictions for tectonically stable areas. Quaternary Science Reviews 24, 1969–1988.

Le Roux, G., Veron, A., Morhange, C., 2003. Geochemical evidences of early anthropogenic activity in harbour sediments from Sidon. Archaeology & history in Lebanon 18, 115–119.

Le Roux, G., Véron, A., Morhange, C., 2005. Lead pollution in the ancient harbours of Marseilles. Méditerranée 31–35.

Martín-Puertas, C., Valero-Garcés, B.L., Mata, M.P., Moreno, A., Giralt, S., Martínez-Ruiz, F., Jiménez-Espejo, F., 2011. Geochemical processes in a Mediterranean Lake: a high-resolution study of the last 4,000 years in Zoñar Lake, southern Spain. J Paleolimnol 46, 405–421.

McLennan, S.M., 2001. Relationships between the trace element composition of sedimentary rocks and upper continental crust. Geochemistry, Geophysics, Geosystems 2, 24.

Ortloff, C.R., Crouch, D.P., 2001. The Urban Water Supply and Distribution System of the Ionian City of Ephesos in the Roman Imperial Period. Journal of Archaeological Science 28, 843–860.

Passchier, C.W., Wiplinger, G., Güngör, T., Kessener, P., Sürmelihindi, G., 2013. Normal fault displacement dislocating a Roman aqueduct of Ephesos, western Turkey. Terra Nova 25, 292–297.

Passchier, C.W., Wiplinger, G., Sürmelihindi, G., Kessener, P., Güngör, T., 2011. Roman aqueducts as indicators of historically active faults in the mediterranean basin. Presented at the 2nd INQUA-IGCP-567 International Workshop on Active Tectonics, Earthquake Geology, Archaeology and Engineering, Corinth, Greece, pp. 186–189.

Pavlopoulos, K., Kapsimalis, V., Theodorakopoulou, K., Panagiotopoulos, I.P., 2012. Vertical displacement trends in the Aegean coastal zone (NE Mediterranean) during the Holocene assessed by geo-archaeological data. The Holocene 22, 717–728.

Rojay, B., Toprak, V., Demirci, C., Süzen, L., 2005. Plio-Quaternary evolution of the Küçük Menderes Graben Southwestern Anatolia, Turkey. Geodinamica Acta 18, 317–331.

Rudnick, R.L., Gao, S., 2003. Composition of the Continental Crust. Treatise on Geochemistry 3, 1–64.

Scherrer, P., 1995. The city of Ephesos: from the roman period to late antiquity, in: Ephesos Metropolis of Asia: An Interdisciplinary Approach to Its Archaeology, Religion, and Culture, Harvard Theological Studies. Helmut Koester, Trinity press international, pp. 1–25.

Somay, A.M., Gemici, Ü., Filiz, S., 2008. Hydrogeochemical investigation of Küçük Menderes River coastal wetland, Selçuk–Izmir, Turkey. Environ Geol 55, 149–164.

Somay, A.M., Gemici, Ü., 2009. Assessment of the Salinization Process at the Coastal Area with Hydrogeochemical Tools and Geographical Information Systems (GIS): Selçuk

Plain, Izmir, Turkey. Water Air Soil Pollut 201, 55–74.
Stanley, J.-D., Carlson, R.W., Van Beek, G., Jorstad, T.F., Landau, E.A., 2007. Alexandria, Egypt, before Alexander the Great: A multidisciplinary approach yields rich discoveries. GSA Today 17, 4–10.

Stock, F., Pint, A., Horejs, B., Ladstätter, S., Brückner, H., 2013. In search of the harbours: New evidence of Late Roman and Byzantine harbours of Ephesus. Quaternary International 312, 57–69.

Stock, F., Kerschner, M., Kraft, J.C., Pint, A., Frenzel, P., Brückner, H., 2014. The palaeo-geographies of Ephesos (Turkey), its harbours and the Artemision - a geoarchaeological reconstruction for the timespan 1500 - 300 BC. Zeitschrift für Geomorphologie.

Stock, F., Knipping, M., Pint, A., Heiss, A.G., Laermanns, H., Mitchell, P., Urz, R., Steskal, M., Wennrich, V., Delile, H., Thanheiser, U., Ployer, R., Rathmayr, E., Ladstätter, S., Brückner, H., submitted. Human impact in the Roman Harbour of Ephesos. The Holocene.

Strabo, 1924. Geography, Loeb Classical Library. Cambridge.

Tacitus, 2009. Annals; http://classics.mit.edu/Tacitus/annals.html.

Vannucci, G., Pondrelli, S., Argnani, A., Morelli, A., Gasperini, P., Boschi, E., 2004. An atlas of Mediterranean seismicity. Ann. Geophys. 47, 247–306.Véron, A.J., Flaux, C., Marriner, N., Poirier, A., Rigaud, S., Morhange, C., Empereur, J.-Y., 2013. A 6000-year geochemical record of human activities from Alexandria (Egypt). Quaternary Science Reviews 81, 138–147.

Véron, A., Goiran, J.P., Morhange, C., Marriner, N., Empereur, J.Y., 2006. Pollutant lead reveals the pre-Hellenistic occupation and ancient growth of Alexandria, Egypt. Geophysical Research Letters 33, 1–4.

Véron, A., Flaux, C., Marriner, N., Poirier, A., Rigaud, S., Morhange, C., Empereur, J.-Y., 2013. A 6000-year geochemical record of human activities from Alexandria (Egypt). Quaternary Science Reviews 81, 138–147.

Vetters, W., 1989. Geologische Übersichtskarte der Umgebung von Ephesus.

Vliegenthart, F.J.L., Sargin, A.H., Gorkmen, A., Dogdu, M.S., 2007. A new approach for groundwater management in Turkey. International congress on river basin management, pp. 64–79.

Wiplinger, G., 2013. Der Değirmendere Aquädukt von Ephesos und seine Zukunft (Wissenschaftlicher Jahresbericht des Österreichischen Archäologischen Instituts No. 24), Babesch, Annual Papers on Mediterranean Archaeoly. Österreichisches Archäologisches Institut, Wien.

Yang, S.Y., Jung, H.S., Choi, M.S., Li, C.X., 2002. The rare earth element compositions of the Changjiang (Yangtze) and Huanghe (Yellow) river sediments. Earth and Planetary Science Letters 201, 407–419.

Zabehlicky, H., 1995. Preliminary Views of the Ephesian Harbor, in: Ephesos – Metropolis of Asia. An Interdisciplinary Approach to Its Archaeology, Religion, and Culture, Harvard Theological Studies. Koester, H.,, Cambridge, Massachusetts, pp. 201–216.

Zhang, C., Wang, L., Zhang, S., Li, X., 1998. Geochemistry of rare earth elements in the mainstream of the Yangtze River, China. Applied Geochemistry 13, 451–462.

Figure captions (see below for figs)

Fig. 1. Map of the Küçük Menderes graben located on the Aegean coast of Turkey (inset) with successive positions of the shorelines and site of core EPH 276 (from Brückner, 2005, modified by Stock et al., 2013 and this study).

Fig. 2. Factor analysis of major and trace element concentrations. Based on Principal Component Analysis, the number of factors is limited to three. (A) Component loadings. The first factor F1 shows the trade-off between an (Al, Ti)-rich detrital component (F1>0) and a Ca-rich carbonate component (F1<0). The second factor F2 is dominated by metals (Ag, Pb, Cu, Mo) and sulfur and shows the effect of anoxia. The third factor F3 is dominated by the light rare-earth elements La and Ce and testifies to the presence of heavy minerals in sand. (B) Distribution of the different factors with depth in the column. The plots are compared with the sedimentary units and the age-depth model.

Fig. 3. (A) Stratigraphy and sedimentology of core EPH 276 showing grain size distribution and environmental facies. (B) Plot of the grain size 99 percentile (D 99) versus the median size (D 50) for the different samples analyzed. The different color groups correspond to different sedimentation regimes (see legend).

Fig. 4. Age-depth model for core EPH 276 deduced from the six ^{14}C dates with ranges calculated using the Clam software (Blaauw, 2010). The size of the data symbols reflects the confidence level.

Fig. 5. Periodogram of magnetic susceptibility in core EPH 276 between 440 and 1100 cm. Mean sampling interval is generally ~1 cm. Four extreme values corresponding to discontinuities were removed from the data set. A fourth-order polynomial was then fitted to the data to remove the long-term trend. Peaks correspond to dominant periods, with confidence levels P in percent in parentheses. We consider that the shortest periods with $P \geq 95\%$ correspond to dominant annual varves, while longer periods correspond to climatic effects or to de-trending artifacts. The periodogram is interpreted as indicating an average sedimentation rate of 20 cm per year.

Fig. 6: Downcore variations of calcium and metal concentrations normalized to aluminum. White- and grey-shaded bands delineate the stratigraphic units A–E, with unit A being deepest and unit E shallowest. Note the discontinuities at ~1080 and ~550 cm depth, notably the increase in S and chalcophile elements at the latter.

Fig. 7. Downcore variations of calcium and metal concentrations normalized to sulfur (see caption of Fig. 4 for details). Two major discontinuities are again observed at ~1080 and ~550 cm depth, which attest to sudden changes in sediment oxygenation. The 1080 cm discontinuity reflects the improved oxygenation of the harbor in the early 1st century AD. Most elements show a negative excursion between 550 and 520 cm indicating that the rise in sulfur precedes the rise in Ca and most other metals; exceptions are Zn and Co, which are in phase with S. Although a slow trend towards anoxia can be seen in sediments below the 550 cm level, the rate of ventilation is greatly reduced after this episode.

Fig. 8. Downcore variations of Pb/Al_{norm}, T_{mod}, μ ($^{238}U/^{204}Pb$), and κ (Th/U) compared with variations in Ca/Al and Mo/Al. Pb/Al is normalized to the upper continental crust average of McLennan (2001). Major T_{mod} discontinuities are observed between units C and D, and at the base of unit E. A major discontinuity in both μ and κ is observed between units A and B. The

variability within unit E reflects an anthropogenic component of uncertain origin.

Table captions

Table 1. Depth range of the sedimentary units and probable age assignment.

Supplementary figure caption

Fig. S1. Abundances of the first-row transition elements (left) and of other metals (right) normalized to the upper crust average of Rudnick and Gao (2003). The different panels correspond to the five sedimentary units (A to E) as identified by sedimentology. Units B and C are smooth, which indicates the predominance of detrital input. Unit A and, to a much greater extent, units D and E show excesses of Mo, Pb, and Ag, which reflect the prevalence of anoxic conditions. Units D and E also show excesses of Cr and Cu. In unit E, the decoupling of Pb from the other elements attests to the addition of anthropogenic Pb (likely present-day gasoline).

Supplementary table captions

Table S1. Major and trace element data for the core samples.

Table S2. Lead isotope data for the core samples.

Table S3. Radiocarbon results for core EPH 276.

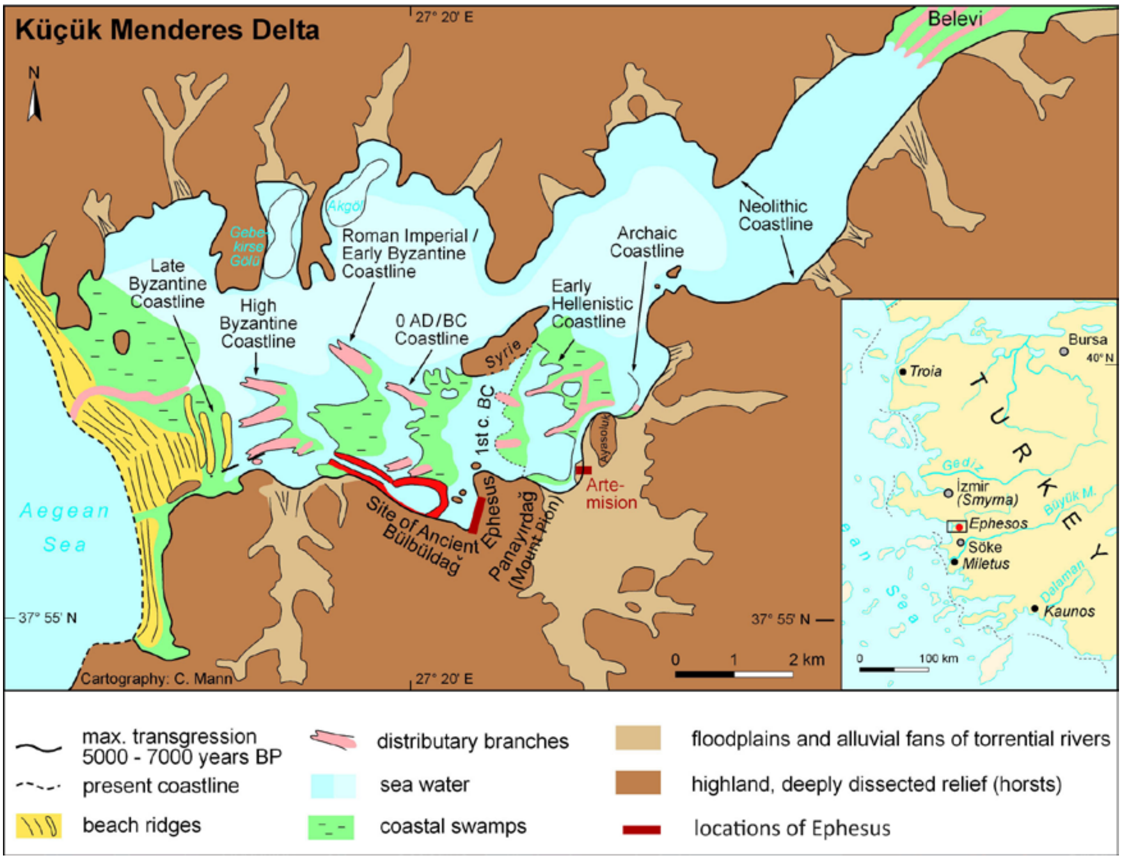

Küçük Menderes Delta
27° 20' E
N
Belevi
Neolithic Coastline
Archaic Coastline
Roman Imperial / Early Byzantine Coastline
Akgöl
Gebe-kirse Gölü
Late Byzantine Coastline
High Byzantine Coastline
0 AD/BC Coastline
Early Hellenistic Coastline
Syrie
1st c. BC
Ayasoluk
Arte-mision
Ephesus
Site of Ancient Bülbüldağ
Panayırdağ (Mount Pion)
Aegean Sea
37° 55' N
37° 55' N
0 1 2 km
Cartography: C. Mann
27° 20' E
Bursa
40° N
Troia
TURKEY
Gediz
İzmir (Smyrna)
Ephesos
Büyük M.
Söke
Miletus
Dalaman
Kaunos
0 100 km
max. transgression 5000 - 7000 years BP
present coastline
beach ridges
distributary branches
sea water
coastal swamps
floodplains and alluvial fans of torrential rivers
highland, deeply dissected relief (horsts)
locations of Ephesus

Fig1

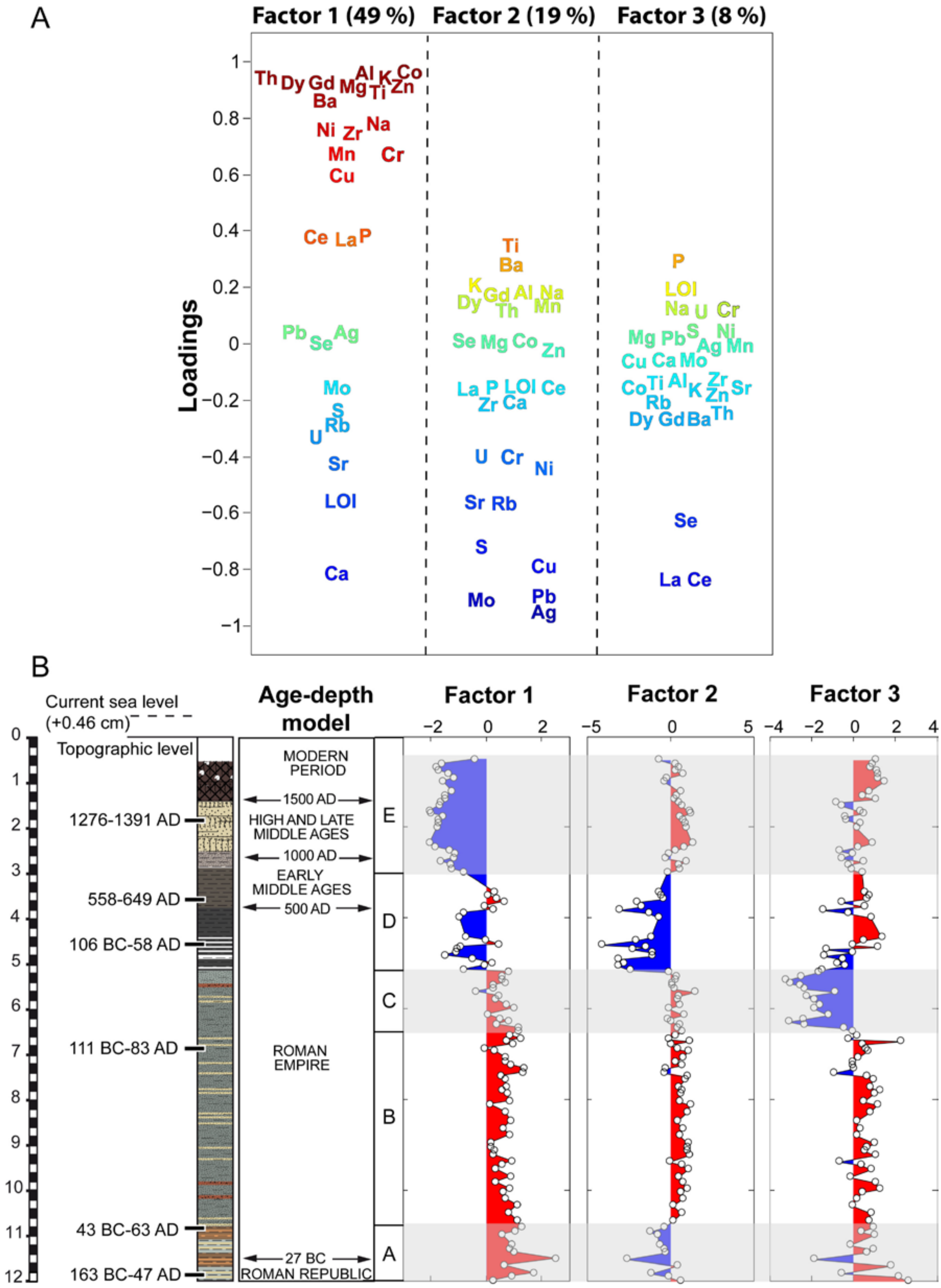
A
Factor 1 (49 %)
Factor 2 (19 %)
Factor 3 (8 %)
Loadings
B
Current sea level (+0.46 cm)
Topographic level
Age-depth model
Factor 1
Factor 2
Factor 3
1276-1391 AD
558-649 AD
106 BC-58 AD
111 BC-83 AD
43 BC-63 AD
163 BC-47 AD
MODERN PERIOD
1500 AD
HIGH AND LATE MIDDLE AGES
1000 AD
EARLY MIDDLE AGES
500 AD
ROMAN EMPIRE
27 BC
ROMAN REPUBLIC
E
D
C
B
A

Fig. 2

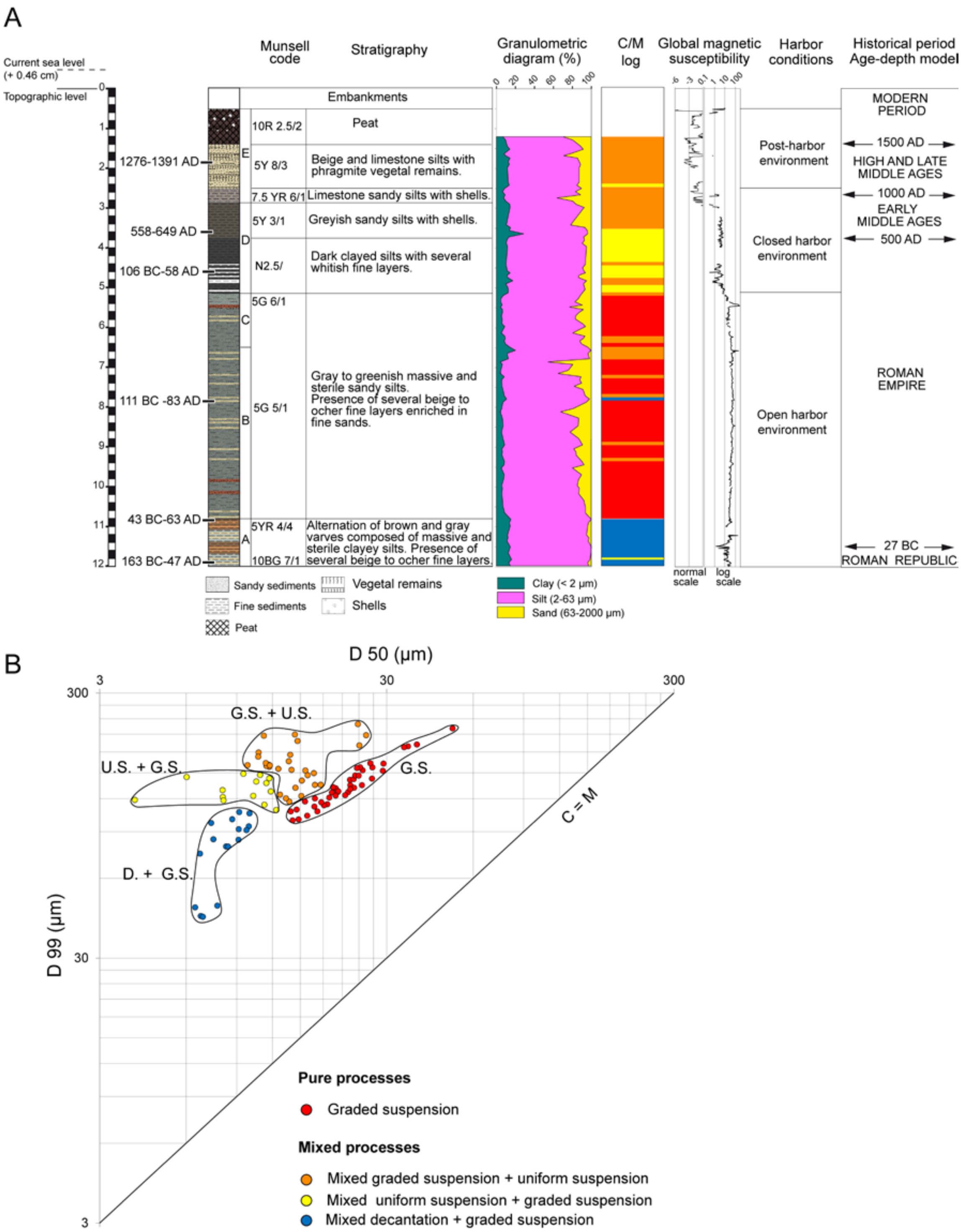
A
Current sea level (+ 0.46 cm)
Topographic level
Munsell code
Stratigraphy
Granulometric diagram (%)
C/M log
Global magnetic susceptibility
Harbor conditions
Historical period Age-depth model
1276-1391 AD
558-649 AD
106 BC-58 AD
111 BC -83 AD
43 BC-63 AD
163 BC-47 AD
Embankments
10R 2.5/2
Peat
5Y 8/3
Beige and limestone silts with phragmite vegetal remains.
7.5 YR 6/1
Limestone sandy silts with shells.
5Y 3/1
Greyish sandy silts with shells.
N2.5/
Dark clayed silts with several whitish fine layers.
5G 6/1
5G 5/1
Gray to greenish massive and sterile sandy silts. Presence of several beige to ocher fine layers enriched in fine sands.
5YR 4/4
10BG 7/1
Alternation of brown and gray varves composed of massive and sterile clayey silts. Presence of several beige to ocher fine layers.
Post-harbor environment
Closed harbor environment
Open harbor environment
MODERN PERIOD
1500 AD
HIGH AND LATE MIDDLE AGES
1000 AD
EARLY MIDDLE AGES
500 AD
ROMAN EMPIRE
27 BC
ROMAN REPUBLIC
normal scale
log scale
Sandy sediments
Fine sediments
Peat
Vegetal remains
Shells
Clay (< 2 µm)
Silt (2-63 µm)
Sand (63-2000 µm)
B
D 50 (µm)
D 99 (µm)
G.S. + U.S.
U.S. + G.S.
G.S.
D. + G.S.
C = M
Pure processes
Graded suspension
Mixed processes
Mixed graded suspension + uniform suspension
Mixed uniform suspension + graded suspension
Mixed decantation + graded suspension

Fig. 3

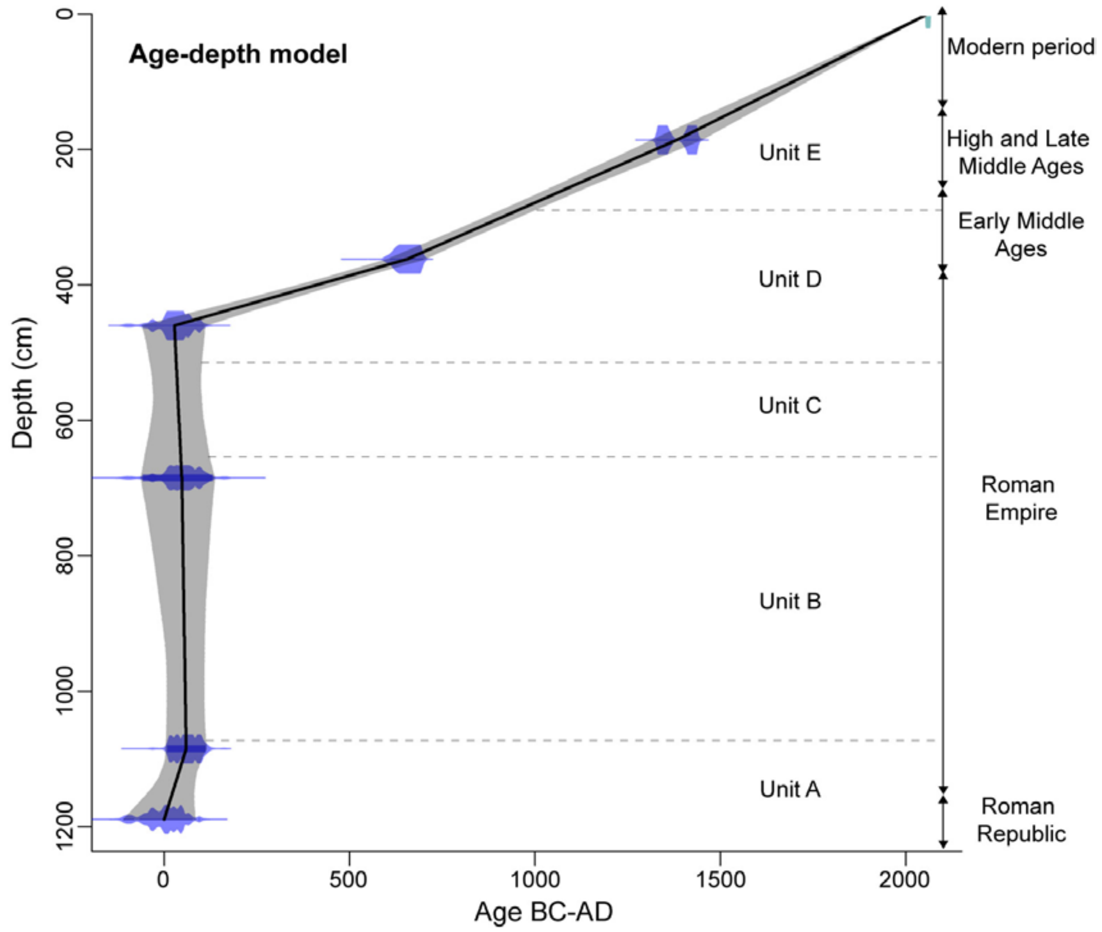

Age-depth model
Depth (cm)
Age BC-AD
Unit E
Unit D
Unit C
Unit B
Unit A
Modern period
High and Late Middle Ages
Early Middle Ages
Roman Empire
Roman Republic

Fig. 4

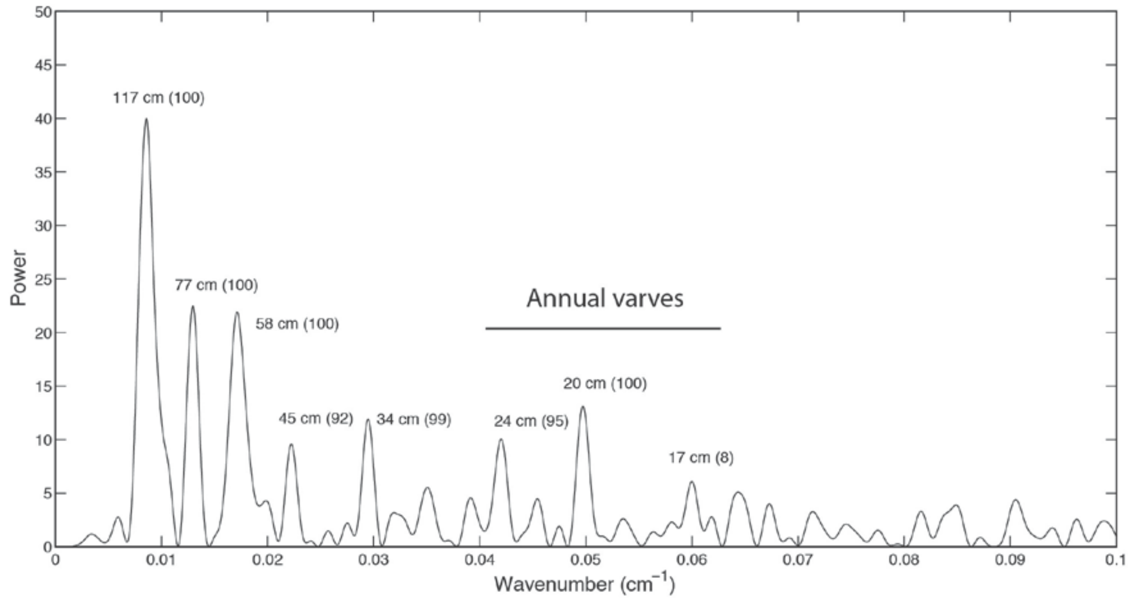

Power
Wavenumber (cm^{-1})
117 cm (100)
77 cm (100)
58 cm (100)
45 cm (92)
34 cm (99)
24 cm (95)
20 cm (100)
17 cm (8)
Annual varves

Fig. 5

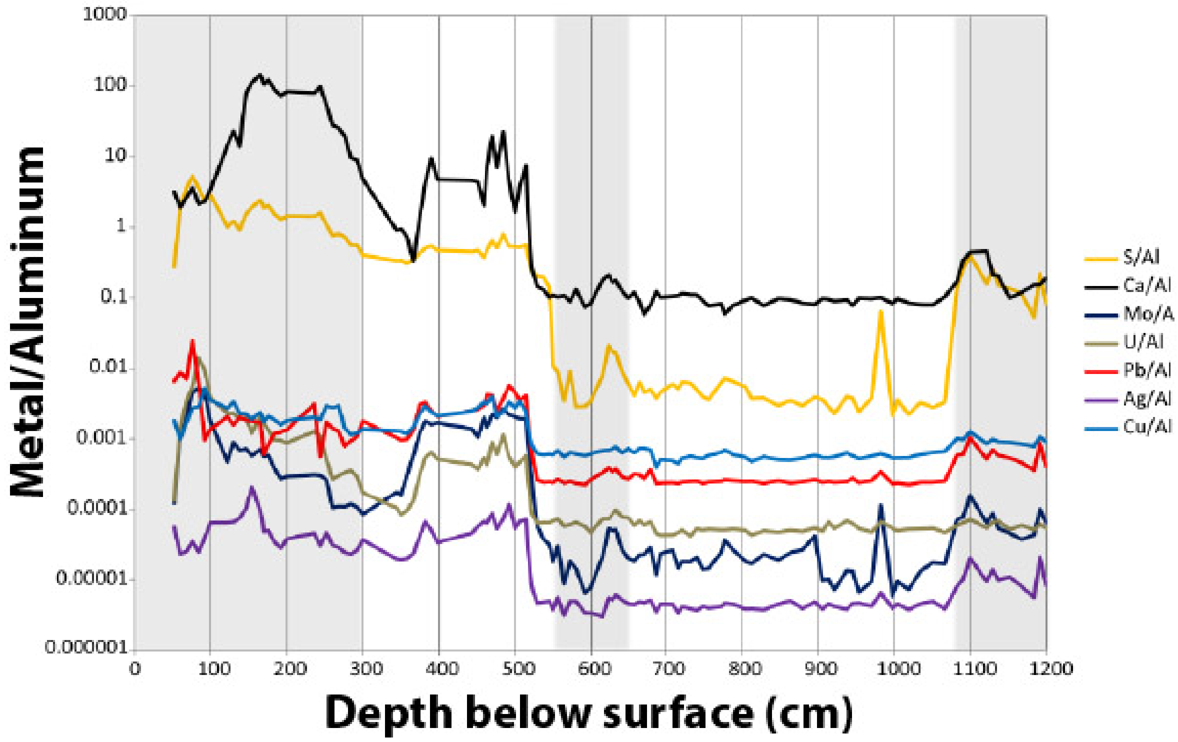

Metal/Aluminum
Depth below surface (cm)
1000
100
10
1
0.1
0.01
0.001
0.0001
0.00001
0.000001
0
100
200
300
400
500
600
700
800
900
1000
1100
1200
S/Al
Ca/Al
Mo/A
U/Al
Pb/Al
Ag/Al
Cu/Al

Fig. 6

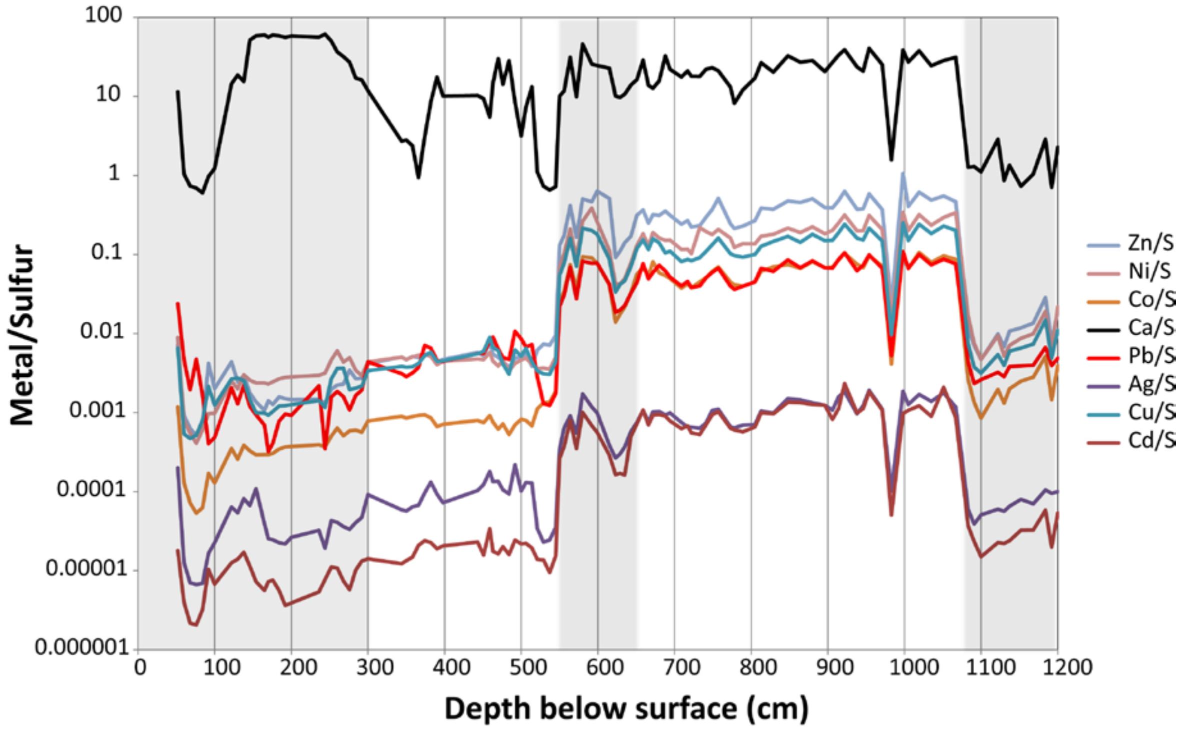

Metal/Sulfur
Depth below surface (cm)
100
10
1
0.1
0.01
0.001
0.0001
0.00001
0.000001
0
100
200
300
400
500
600
700
800
900
1000
1100
1200
Zn/S
Ni/S
Co/S
Ca/S
Pb/S
Ag/S
Cu/S
Cd/S

Fig. 7

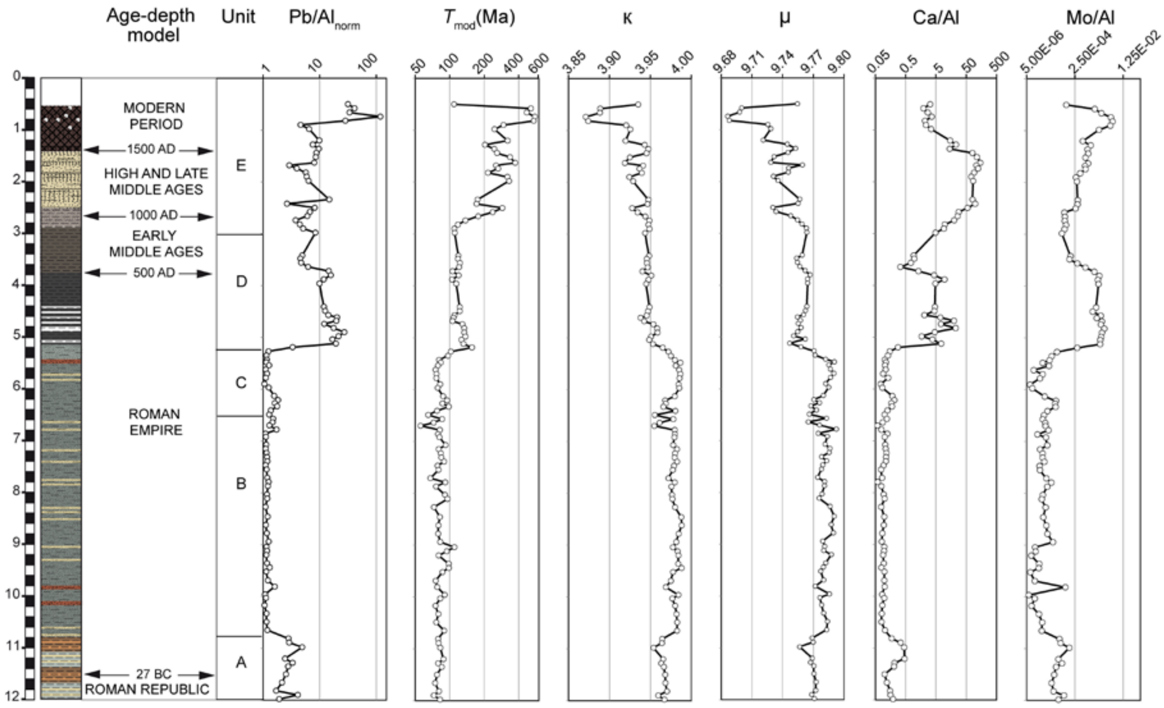

Fig. 8

Unit	Depth (cm)	Probable Age
A	1200-1070	Roman Republic
B	1070-650	Early Roman Empire
C	650-515	Late Roman Empire
D	515-300	Early Byzantine (4th-8th century)
E	300-0	Late Byzantine and Turkish

Table 1 : Depth range of the sedimentary units and probable age assignment.

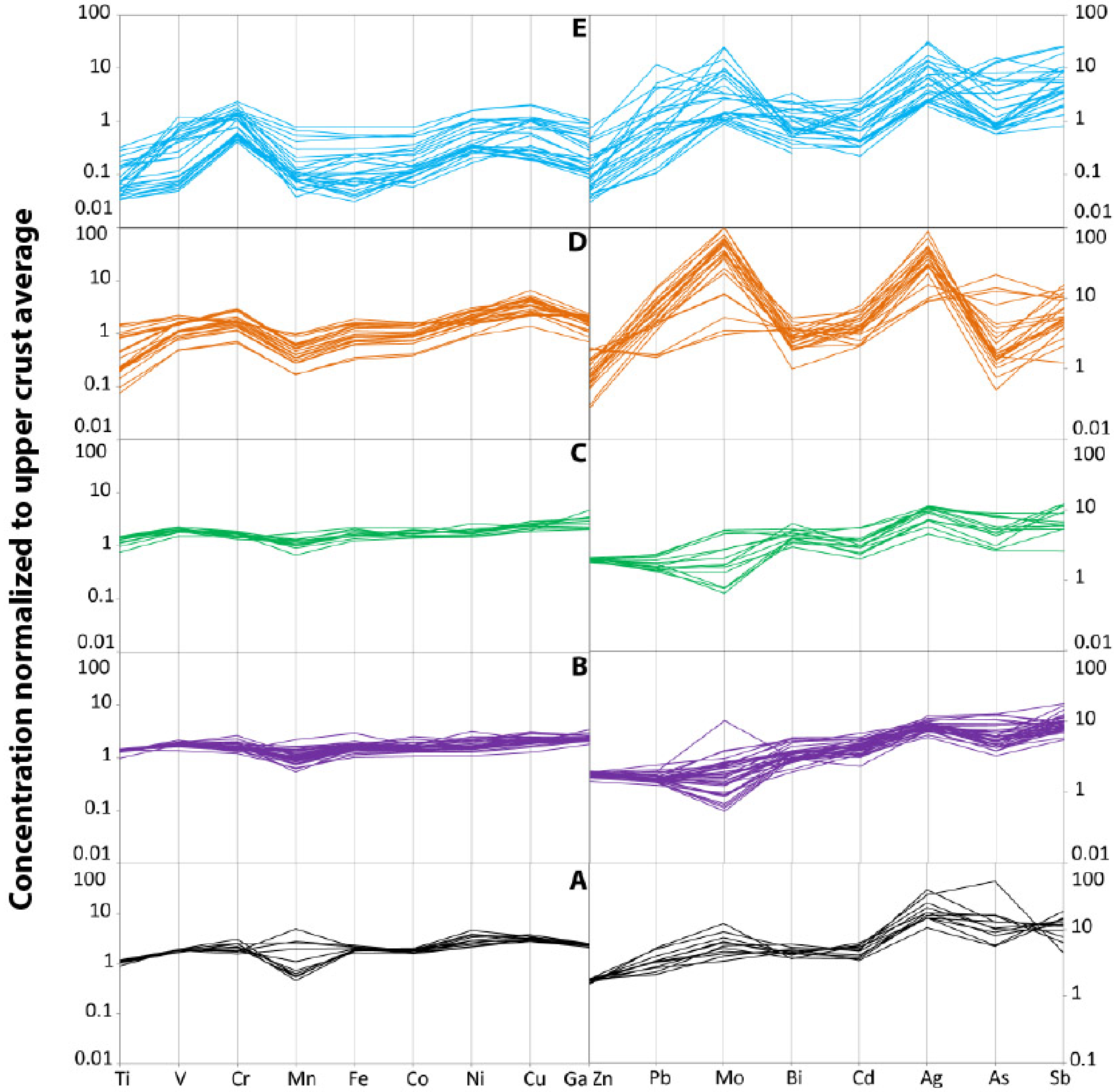
Concentration normalized to upper crust average
E
D
C
B
A
100
10
1
0.1
0.01
Ti
V
Cr
Mn
Fe
Co
Ni
Cu
Ga
Zn
Pb
Mo
Bi
Cd
Ag
As
Sb

Fig. S1

777

Table S1. Major elements are in wt.% and trace elements are in ppm.

Lab code	Depth (cm)	Unit	Al_2O_3	CaO	Fe_2O_3	K_2O	MgO	MnO	Na_2O	P_2O_5	SO_3	TiO_2	LOI	Zr	Li	Be	V	Ga	Se	Rb	Sr	Y	Mo	Ba	La	Ce	Nd	Sm	Eu	Gd	Dy	Er	Yb	Lu	Th	U	Pb	Ag	Cr
129L	50	E	5.69	13.49	2.73	0.92	2.19	0.041	0.82	0.26	1.68	0.08	82.97	33.67	19.20	0.85	61.04	7.87	2.34	78.05	199.01	10.46	3.70	151.85	14.34	28.74	12.13	2.53	0.56	2.42	2.14	1.11	1.03	0.16	2.89	4.09	200.74	1.678	130.64
128L	58	E	1.51	2.14	0.56	0.35	1.06	0.009	0.91	0.15	2.92	0.09	87.61	15.15	3.26	0.22	38.82	2.21	9.44	28.56	83.56	1.51	9.89	56.68	3.76	6.96	2.71	0.47	0.11	0.49	0.34	0.18	0.19	0.03	0.71	11.60	69.30	0.186	71.10
127L	66	E	0.88	1.74	0.48	0.18	0.87	0.005	0.69	0.16	3.38	0.04	87.63	9.15	1.50	0.15	42.42	1.21	7.62	19.00	63.88	1.16	9.94	30.02	2.12	4.10	1.64	0.31	0.06	0.33	0.25	0.14	0.14	0.02	0.42	16.22	33.02	0.119	123.06
126L	74	E	0.67	1.80	0.41	0.15	0.93	0.005	1.10	0.15	3.71	0.03	85.49	11.95	0.91	0.11	42.26	0.77	7.49	17.17	62.26	0.84	16.12	26.70	1.41	2.74	1.11	0.19	0.05	0.23	0.18	0.10	0.10	0.01	0.28	19.57	87.74	0.124	69.59
125L	82	E	1.00	1.60	0.47	0.19	0.84	0.004	0.91	0.17	3.80	0.06	74.10	21.28	2.56	0.17	87.12	1.37	3.27	18.02	59.52	1.47	27.66	25.31	2.49	4.84	1.97	0.36	0.08	0.41	0.33	0.15	0.15	0.02	0.40	73.88	31.72	0.132	122.00
124L	90	E	1.14	1.96	1.35	0.21	0.76	0.008	0.81	0.29	2.88	0.04	54.03	19.42	2.68	0.21	118.02	1.66	4.24	22.34	74.78	1.72	26.53	34.33	3.35	6.32	2.44	0.43	0.09	0.43	0.35	0.19	0.18	0.03	0.58	56.37	5.85	0.239	94.60
123L	98	E	1.18	3.05	0.95	0.22	0.79	0.007	0.89	0.38	3.56	0.05	6.29	25.10	2.15	0.20	66.70	1.66	9.17	25.39	86.17	2.12	10.98	44.69	3.03	6.18	2.61	0.52	0.11	0.52	0.43	0.23	0.23	0.04	0.54	23.59	8.62	0.402	159.64
122L	120	E	2.08	22.57	1.36	0.38	0.99	0.013	0.67	0.55	2.23	0.02	8.06	25.03	5.26	0.38	72.54	2.90	3.32	96.49	359.54	4.10	5.19	100.71	6.06	12.07	5.16	0.97	0.22	1.02	0.80	0.44	0.39	0.06	0.97	25.49	22.86	0.711	191.95
121L	128	E	1.54	26.02	0.57	0.26	0.94	0.008	0.60	0.38	2.00	0.03	11.40	19.44	3.27	0.27	61.92	2.12	2.76	111.41	428.67	2.72	7.27	96.46	4.36	8.75	3.67	0.74	0.18	0.78	0.61	0.33	0.30	0.05	0.70	18.69	12.93	0.538	103.37
120L	136	E	2.30	24.04	0.97	0.42	1.25	0.012	0.68	0.19	2.22	0.08	5.09	23.48	8.09	0.33	52.07	3.32	7.75	135.18	499.48	4.25	8.42	123.27	5.91	11.60	5.00	1.03	0.24	1.07	0.88	0.47	0.40	0.07	1.02	23.19	24.73	0.909	117.05
119L	144	E	0.75	44.22	0.33	0.14	1.57	0.011	0.33	0.10	1.22	0.04	16.23	13.94	2.14	0.14	8.62	1.02	2.45	192.63	775.47	1.48	2.88	103.87	2.13	4.08	1.82	0.37	0.12	0.41	0.32	0.17	0.18	0.05	0.65	7.89	7.33	0.408	43.00
118L	152	E	0.54	45.05	0.22	0.10	1.61	0.007	0.31	0.07	1.10	0.03	22.04	21.52	0.42	0.10	5.31	0.63	11.13	178.07	720.24	0.90	1.65	90.08	1.29	2.63	1.20	0.23	0.07	0.24	0.21	0.11	0.10	0.02	0.36	3.46	5.17	0.601	42.52
117L	163	E	0.41	44.78	0.17	0.08	1.46	0.005	0.35	0.08	1.07	0.02	21.13	22.55	1.88	0.09	4.66	0.50	13.52	242.51	983.45	0.97	1.57	105.22	1.00	2.03	0.89	0.20	0.05	0.19	0.16	0.09	0.10	0.01	0.34	4.54	3.72	0.210	37.15
116L	168	E	0.54	43.13	0.24	0.10	1.33	0.007	0.38	0.12	1.09	0.02	17.83	19.90	4.46	0.11	6.33	0.71	14.02	230.81	931.75	0.93	1.61	107.27	1.41	3.00	1.24	0.24	0.07	0.26	0.20	0.11	0.11	0.02	0.33	4.64	1.76	0.139	46.72
115L	174	E	0.49	44.18	0.20	0.09	1.43	0.007	0.33	0.09	1.05	0.02	15.68	16.93	2.66	0.10	5.10	0.60	13.56	181.65	736.25	0.94	1.51	94.11	1.41	2.88	1.25	0.24	0.06	0.25	0.21	0.09	0.09	0.01	0.28	3.46	2.15	0.129	40.37
114L	182	E	0.65	43.60	0.27	0.12	1.44	0.008	0.36	0.09	1.06	0.03	20.08	24.98	2.29	0.12	6.45	0.84	6.44	170.08	680.71	1.34	1.31	84.67	1.68	3.45	1.49	0.29	0.07	0.30	0.27	0.16	0.12	0.02	0.30	3.37	4.15	0.120	48.21
113L	190	E	0.80	43.09	0.36	0.14	1.39	0.008	0.37	0.07	1.10	0.03	21.17	19.00	1.71	0.14	7.32	1.12	15.84	216.87	870.19	1.74	1.14	96.74	2.24	4.68	1.93	0.36	0.10	0.36	0.36	0.19	0.15	0.03	0.42	4.02	5.28	0.120	55.35
112L	198	E	0.69	43.10	0.33	0.13	1.43	0.008	0.36	0.07	1.06	0.03	21.67	10.53	2.95	0.14	6.99	0.92	11.25	194.90	776.86	1.23	1.07	88.64	2.00	4.03	1.72	0.34	0.08	0.35	0.29	0.15	0.13	0.02	0.36	3.23	4.90	0.140	53.34
111L	234	E	0.73	43.58	0.40	0.13	1.36	0.010	0.41	0.08	1.11	0.04	21.30	18.41	2.32	0.12	8.99	0.96	14.19	258.41	1040.35	1.56	1.20	102.14	2.06	4.26	1.80	0.41	0.10	0.38	0.29	0.15	0.16	0.02	0.38	4.95	12.08	0.179	49.58
110L	242	E	0.61	44.49	0.27	0.12	1.51	0.008	0.38	0.06	1.03	0.02	15.59	14.49	2.56	0.10	5.85	0.73	11.99	226.73	916.28	1.06	0.99	93.08	1.57	3.28	1.34	0.26	0.07	0.28	0.23	0.12	0.10	0.02	0.29	3.58	1.81	0.100	53.11
109L	250	E	1.08	44.08	0.58	0.20	1.51	0.010	0.34	0.06	1.25	0.05	37.17	13.45	3.59	0.21	10.95	1.52	13.26	176.21	693.93	2.91	1.50	94.28	3.90	7.98	3.34	0.68	0.18	0.70	0.60	0.31	0.27	0.07	1.10	2.94	9.89	0.269	97.00
108L	258	E	2.06	42.64	1.16	0.35	1.77	0.017	0.40	0.07	1.66	0.09	17.51	31.06	8.33	0.32	19.78	2.97	18.00	183.78	700.52	4.98	1.15	105.94	6.69	14.26	5.84	1.14	0.27	1.24	1.04	0.50	0.47	0.08	1.43	2.92	15.43	0.341	135.37
107L	266	E	2.22	42.23	1.33	0.36	1.61	0.021	0.44	0.08	1.89	0.09	21.12	26.53	13.68	0.42	19.96	3.28	7.20	196.99	759.74	5.71	1.29	106.89	8.06	17.00	6.91	1.40	0.31	1.47	1.19	0.61	0.59	0.09	1.59	3.53	14.99	0.340	124.42
106L	274	E	2.69	39.70	1.66	0.42	1.62	0.030	0.52	0.11	2.09	0.11	22.24	29.03	13.97	0.43	26.00	3.87	9.03	234.90	899.95	6.52	1.55	121.01	9.14	19.21	7.95	1.59	0.38	1.63	1.36	0.70	0.62	0.10	1.85	4.73	11.34	0.350	123.47
105L	282	E	4.87	35.08	2.79	0.76	1.48	0.053	0.68	0.12	2.93	0.14	22.06	25.37	22.38	0.76	45.24	7.00	4.57	332.65	1288.72	11.26	3.10	174.75	15.32	30.98	13.17	2.71	0.61	2.73	2.23	1.10	0.99	0.17	3.01	9.15	24.20	0.597	136.95
104L	290	E	5.34	35.78	3.08	0.86	1.38	0.068	0.70	0.14	3.16	0.18	22.20	35.32	24.01	0.87	46.22	7.92	8.09	419.18	1643.21	12.40	3.03	192.59	17.69	35.79	15.14	3.01	0.67	3.17	2.68	1.33	1.19	0.19	3.44	8.28	30.55	0.746	148.51
103L	298	E	7.93	28.21	4.51	1.35	2.15	0.078	0.83	0.09	3.40	0.20	13.18	27.47	42.69	1.29	77.73	12.82	4.47	368.83	1347.50	17.77	3.62	240.72	25.57	51.11	21.79	4.41	0.97	4.50	3.74	1.96	1.78	0.28	5.12	7.18	74.67	1.558	215.36
102L	342	D	13.80	9.32	7.62	2.50	3.30	0.063	1.21	0.19	4.89	0.56	13.96	45.91	71.29	2.35	140.88	22.55	4.90	194.76	433.30	27.37	12.68	357.76	43.05	84.84	37.40	7.45	1.64	7.63	6.13	3.06	2.69	0.42	8.47	7.65	75.90	1.437	264.33
101L	348	D	14.66	10.34	7.68	2.53	3.33	0.065	1.24	0.17	5.24	0.52	13.75	71.00	75.62	2.22	140.08	22.34	2.69	235.63	596.11	28.20	12.32	354.58	43.66	82.06	38.25	7.50	1.67	7.73	6.19	3.10	2.75	0.43	8.55	6.59	74.83	1.490	256.78
100L	356	D	15.45	8.46	8.10	2.66	3.52	0.060	1.35	0.22	5.09	0.61	15.79	72.21	76.37	2.36	148.11	23.23	6.22	206.11	455.83	27.68	24.70	364.23	44.58	83.62	38.69	7.81	1.68	7.85	6.19	3.08	2.74	0.44	8.67	7.88	81.03	1.633	261.41
99L	364	D	14.65	3.60	7.92	2.71	3.38	0.061	1.57	0.16	5.46	0.53	17.71	73.80	80.26	2.54	153.21	24.34	3.51	143.55	189.55	28.85	44.60	335.66	45.89	85.86	40.21	7.96	1.76	8.14	6.50	3.24	2.91	0.50	9.93	10.25	101.94	1.837	277.76
98L	372	D	10.53	10.23	7.07	2.07	3.07	0.059	1.49	0.18	4.78	0.29	21.43	56.90	56.70	2.05	148.48	19.82	3.90	202.17	524.98	26.73	66.45	306.27	38.68	78.98	33.56	6.86	1.49	7.06	5.70	2.91	2.63	0.44	7.54	16.85	169.66	2.296	242.69
97L	380	D	7.76	24.75	5.46	1.53	2.39	0.047	1.33	0.22	4.15	0.14	20.53	53.27	42.70	1.50	110.09	14.78	9.47	557.84	2188.98	21.39	73.50	264.51	29.95	61.71	25.83	5.15	1.17	5.49	4.48	2.35	2.16	0.34	5.78	22.38	136.33	2.734	179.67
96L	388	D	5.88	41.56	3.47	0.94	1.50	0.028	0.96	0.24	3.39	0.13	18.81	35.61	30.71	1.04	74.78	9.15	7.52	1105.43	4623.97	15.29	50.05	193.91	20.20	41.95	17.70	3.42	0.76	3.69	3.08	1.64	1.47	0.24	3.70	20.03	77.45	1.575	103.72
95L	396	D	8.39	29.64	4.78	1.32	2.05	0.035	1.13	0.22	4.18	0.22	20.18	45.59	41.58	1.43	103.08	13.21	4.55	797.59	3190.14	20.30	74.72	231.07	27.55	56.16	23.23	4.75	1.04	4.91	4.06	2.11	1.98	0.32	5.23	22.73	92.94	1.513	144.44
94L	441	D	8.45	28.94	4.99	1.33	2.13	0.040	1.03	0.19	4.02	0.14	21.98	43.22	38.06	1.37	107.50	13.59	9.29	681.13	2680.54	20.17	62.14	238.44	28.00	57.34	24.24	4.89	1.05	5.05	4.08	2.08	1.88	0.32	5.41	19.34	111.91	2.070	153.70
93L	449	D	8.45	27.47	5.05	1.34	2.47	0.047	1.16	0.20	4.18	0.13	21.97	29.97	35.48	1.40	101.91	12.84	10.31	382.79	1417.27	19.05	47.19	237.42	26.14	54.05	22.34	4.46	1.01	4.64	3.81	2.03	1.85	0.30	4.83	16.49	117.73	2.567	162.71
92L	457	D	10.36	15.80	6.34	1.64	2.79	0.052	1.43	0.20	4.11	0.15	24.15	55.00	54.39	1.68	163.22	16.32	3.96	222.94	661.51	24.92	110.04	273.15	33.75	67.53	27.76	5.59	1.21	5.88	4.74	2.58	2.38	0.39	6.53	29.80	164.69	3.710	191.27
91L	462	D	6.85	35.42	4.12	1.09	1.83	0.035	1.09	0.25	3.43	0.15	21.71	39.70	29.16	1.15	86.82	10.95	8.25	741.76	2972.35	15.45	52.96	277.42	23.64	46.16	19.53	3.89	0.86	4.02	3.22	1.69	1.52	0.23	4.49	15.52	154.05	2.302	120.99
90L	468	D	3.34	48.60	2.00	0.53	1.00	0.017	0.91	0.25	2.30	0.05	22.51	27.34	15.19	0.60	48.03	5.29	11.63	1274.51	5435.99	9.07	39.26	262.26	11.96	23.78	9.90	1.97	0.47	2.10	1.77	0.94	0.90	0.14	2.06	15.86	73.49	1.551	65.80
89L	474	D	6.58	35.40	3.95	1.04	1.70	0.031	1.14	0.19	3.55	0.14	18.86	48.16	28.44	1.20	88.57	10.64	25.04	930.49	3821.69	15.44	70.65	291.04	22.64	46.13	19.10	3.76	0.91	3.98	3.34	1.74	1.64	0.29	4.89	21.40	88.14	1.877	128.99
88L	482	D	2.99	49.65	1.82	0.47	0.89	0.017	0.93	0.23	2.50	0.06	23.81	18.54	12.18	0.54	46.68	4.78	18.53	1348.12	5759.46	8.11	42.16	308.47	10.69	21.47	9.00	1.81	0.46	1.89	1.57	0.85	0.75	0.13	1.96	17.75	58.84	1.172	61.09
87L	490	D	7.48	25.17	4.25	1.13	1.77	0.035	1.35	0.21	4.27	0.12	19.22	49.35	30.56	1.18	104.42	11.39	19.08	667.57	2673.63	19.26	87.63	392.41	28.37	54.93	22.93	4.57	1.06	4.77	3.99	2.08	1.84	0.30	5.18	22.16	227.78	4.666	135.63
86L	498	D	10.05	12.46	7.01	1.94	2.39	0.054	1.67	0.19	5.63	0.30	23.74	54.17	59.56	1.91	156.69	19.22	19.39	315.61	1005.12	29.21	109.73	412.47	45.86	83.84	37.91	7.51	1.70	7.78	6.23	3.31	2.81	0.45	8.23	21.07	241.13	2.873	190.82
85L	504	D	7.65	21.54	4.99	1.50	2.08	0.041	1.25	0.18	4.22	0.14	24.77	50.75	40.52	1.41	112.38	14.39	8.75	499.70	1912.70	20.22	78.47	269.29	29.23	59.90	24.80	5.04	1.12	5.13	4.18	2.19	2.00	0.33	5.55	18.80	143.03	2.756	165.81
84L	512	D	6.24	34.32	3.57	1.00	1.49	0.028	1.09	0.19	3.71	0.09	4.56	39.08	26.47	0.99	79.69	9.57	12.11	972.82	4048.41	14.66	63.22	372.06	22.18	43.81	18.21	3.65	0.86	3.78	3.10	1.49	1.44	0.22	3.93	18.95	134.80	2.385	108.79
83L	519	C	18.17	3.72	8.43	3.30	2.63	0.087	1.60	0.09	4.77	0.68	3.99	59.18	74.73	2.89	183.84	31.34	18.38	202.99	353.25	44.18	28.87	537.21	69.53	134.93	61.79	12.26	2.59	12.54	9.67	4.69	4.09	0.64	12.47	8.84	67.65	0.812	158.86
82L	527	C	19.08	2.10	8.79	3.55	2.78	0.097	1.68	0.09	4.09	0.84	4.57	64.94	78.13	3.14	195.31	34.31	27.53	186.20	247.64	51.55	5.88	733.31	73.77	143.92	67.45	13.68	2.81	13.58	10.86	5.59	4.87	0.80	13.24	6.36	26.65	0.470	154.88
81L	535	C	19.32	1.85	9.06	3.50	2.82	0.096	1.73	0.13	4.02	0.96	7.01	59.18	59.45	2.98	193.74	33.45	17.89	175.49	218.54	46.66	3.87	753.91	73.44	144.33	67.22	13.40	2.79	13.67	10.53	5.18	4.54	0.73	13.17	6.65	24.76	0.491	147.80
80L	543	C	20.06	1.51	10.55	3.49	2.70	0.098	1.64	0.15	3.00	0.92	5.23	56.33	82.14	3.17	213.98	34.29	19.68	172.53	200.17	52.11	3.36	762.22	75.73	148.37	68.76	13.94	2.94	13.95	10.96	5.50	4.71	0.75	13.37	6.88	26.19	0.528	155.32
79L	548	C	18.54	1.51	7.62	3.61	2.80	0.090	1.88	0.16	0.21	0.75	3.72	68.34	58.76	3.13	174.55	34.45	29.76	172.66	198.33	47.18	1.78	816.66	71.66	139.93	65.18	13.25	2.72	13.07	10.26	5.03	4.55	0.75	13.05	6.79	23.60	0.372	158.86
78L	554	C	18.59	1.42	8.57	3.57	2.72	0.120	1.65	0.19	0.17	0.90	5.07	68.27	77.89	3.40	218.23	35.65	22.33	173.88	188.81	52.56	2.98	786.02	75.97	148.63	68.69	13.95	2.86	14.07	11.22	5.55	4.94	0.79	13.47	7.20	26.51	0.552	172.87
ZL	562	C	17.97	1.44	7.04	3.51	2.72	0.067	2.03	0.15	0.07	0.62	5.62	45.95	60.79	2.99	172.79	33.52	23.60	168.85	200.77	42.19	0.84	792.52	64.89	126.58	59.23	11.84	2.54	12.01	9.07	4.35	3.87	0.60	11.10	5.48	22.51	0.300	151.50
77L	570	C	19.14	1.27	8.79	3.59	2.82	0.098	1.79	0.18	0.18	0.97	5.59	56.73	68.92	3.11	218.97	35.75	30.70	173.22	192.92	51.52	1.85	800.02	76.16	150.19	69.53	14.07	2.86	14.19	11.02	5.54	4.83	0.77	13.29	6.20	25.23	0.502	163.57
76L	578	C	18.28	1.78	11.73	3.31	2.96	0.127	1.68	0.24	0.06	0.90	7.44	55.33	63.89	2.90	196.64	32.78	32.53	163.45	189.01	46.16	1.41	792.25	68.89	135.43	62.80	12.64	2.63	12.97	9.94	5.21	4.53	0.72	12.02	6.32	22.83	0.479	155.30
75L	590	C	20.95	1.15	8.78	3.72	2.97	0.104	1.71	0.18	0.06	0.83	6.53	40.42	73.64	3.15	195.06	36.02	23.12	172.05	172.07	47.88	0.72	784.20	74.80	147.79	67.55	13.53	2.77	13.48	10.37	5.16	4.35	0.70	13.07	6.33	24.86	0.379	163.92
74L	597	C	20.62	1.28	10.86	3.47	3.07	0.133	1.45	0.20	0.07	0.73	9.21	56.39	70.24	2.15	192.40	33.94	9.89	157.75	161.05	50.28	0.86	771.76	68.77	135.34	65.78	13.44	2.87	13.33	10.85	5.39	4.82	0.70	12.00	5.17	28.97	0.369	167.41
73L	613	C	14.87	1.98	8.95	3.39	2.60	0.100	1.76	0.16	0.12	0.48	8.33	42.46	60.92	2.00	147.75	31.42	8.81	166.04	241.21	44.94	1.68	788.45	62.25	121.88	60.06	12.41	2.62	12.14	9.68	4.88	4.30	0.60	10.15	5.74	26.12	0.240	140.66
72L	621	C	19.45	3.03	10.05	3.21	2.90	0.101	1.42	0.19	0.43	0.71	8.48	64.69	70.23	2.05	190.13	32.22	5.14	186.09	304.10	54.89	5.50	717.57	73.15	144.90	69.96	14.22	3.03	14.34	11.74	5.94	5.10	0.77	12.81	7.56	39.84	0.572	152.84
71L	627	C	21.16	2.61	9.34	3.32	2.81	0.122	1.54	0.22	0.38	0.95	8.91	49.75	82.02	2.14	208.53	36.31	9.74	193.21	288.02	72.99	5.60	746.15	92.21	190.26	94.94	19.64	3.90	19.62	16.01	7.83	6.75	1.00	16.86	9.65	38.03	0.577	140.50
70L	633	C	18.33	2.40	8.50	3.35	2.67	0.111	1.54	0.20	0.32	0.92	11.20	62.12	73.37	2.06	195.60	35.07	11.90	177.65	241.48	65.78	5.01	742.42	82.44	176.31	84.70	17.69	3.55	17.77	14.26	7.27	6.11	0.89	15.43	9.50	36.39	0.591	135.91
69L	641	C	21.29	1.97	8.56	3.52	2.70	0.120	2.32	0.23	0.20	0.90	11.15	43.17	43.94	3.13	181.79	34.48	10.86	158.49	187.01	64.86	3.01	724.49	22.77	47.03	87.95	17.93	3.82	18.00	14.06	6.80	5.62	0.91	16.99	8.84	32.58	0.582	122.04
68L	649	C	21.03	1.55	12.26	3.18	2.72	0.173	2.21	0.33	0.14	0.85	9.48	36.50	74.26	3.07	191.47	34.15	14.73	141.47	155.31	69.67	2.24	722.50	24.52	50.06	95.37	19.50	4.32	19.54	15.22	7.20	5.96	0.96	16.74	8.48	30.08	0.510	129.96
67L	657	B	19.99	1.77	16.38	3.07	2.59	0.222	1.87	0.36	0.09	0.63	9.48	49.15	70.39	3.00	173.59	30.64	10.74	133.04	137.80	51.61	1.95	693.66	16.98	35.90	63.19	12.84	3.01	12.96	10.56	5.32	4.55	0.76	12.42	6.31	33.60	0.471	123.40
66L	664	B	21.38	1.38	10.48	3.47	2.86	0.141	2.61	0.25	0.14	0.85	13.01	38.42	70.97	3.10	188.59	33.55	8.20	140.55	124.14	58.92	2.54	670.38	21.27	43.78	80.93	16.35	3.66	16.22	12.86	6.05	5.15	0.88	15.83	7.79	35.15	0.549	136.67
65L	670	B	22.41	0.97	9.49	3.26	2.91	0.141	2.43	0.22	0.11	0.85	3.78	47.76	81.27	3.03	210.66	34.65	10.35	138.88	124.05	57.40	2.72	651.79	17.60	37.31	68.44	14.11	3.27	14.36	12.10	6.03	5.42	0.91	12.64	7.11	32.30	0.557	148.71
64L	678	B	21.52	1.25	9.67	3.38	2.83	0.144	2.49	0.23	0.11	0.82	5.53	34.03	52.49	3.26	176.10	32.98	6.92	142.68	109.30	59.50	3.29	656.09	22.75	46.41	85.05	17.11	3.69	17.02	12.74	6.02	5.12	0.85	17.40	7.56	41.64	0.591	119.54
63L	686	B	17.09	1.56	5.76	2.90	2.33	0.065	3.81	0.20	0.07	0.91	4.98	37.31	26.43	2.71	133.72	24.98	4.64	125.55	194.16	31.23	1.07	625.62	12.45	23.53	44.11	8.82	2.09	8.67	6.67	3.30	2.79	0.47	7.88	4.14	21.13	0.318	111.67
62L	692	B	19.49	1.46	7.99	3.50	2.85	0.096	3.19	0.23	0.09	0.90	4.52	39.00	35.54	2.99	170.83	29.75	4.99	144.55	175.28	38.37	2.42	752.87	14.71	30.21	56.01	11.18	2.60	10.99	8.19	3.94	3.33	0.54	10.30	4.47	24.49	0.470	146.16
61L	707	B	20.09	1.58	7.35	3.69	2.99	0.088	3.21	0.19	0.13	0.94	6.06	34.47	35.80	2.90	175.68	30.38	4.68	151.20	193.03	35.93	2.81	766.87	14.18	29.43	54.87	11.03	2.57	10.71	7.81	3.72	3.14	0.56	10.37	4.65	25.50	0.480	150.75
60L	715	B	18.95	1.52	6.44	3.45	2.68	0.063	3.59	0.19	0.10	0.91	5.44	20.98	31.78	2.65	156.68	28.05	3.53	138.99	192.41	34.92	1.48	699.86	13.02	27.41	50.78	10.13	2.36	9.84	7.44	3.64	3.08	0.51	9.43	4.71	23.57	0.340	128.37
59L	723	B	20.23	1.73	11.62	3.62	2.97	0.147	2.88	0.30	0.14	0.85	7.14	44.32	38.97	2.83	174.15	30.05	7.11	147.03	177.73	42.52	1.94	755.76	15.09	31.19	57.43	11.71	2.67	11.59	8.91	4.32	3.70	0.61	10.90	5.44	26.12	0.448	137.49
58L	731	B	20.61	1.69	8.34	3.74	4.11	0.115	2.92	0.18	0.14	0.90	5.62	38.92	39.49	2.92	185.28	30.36	4.58	143.52	166.60	39.67	1.98	698.94	14.54	29.85	54.62	11.01	2.57	10.72	8.30	4.11	3.56	0.58	10.46	4.60	27.17	0.429	244.58
57L	739	B	19.55	1.59	10.41	3.64	3.39	0.133	2.83	0.23	0.10	0.85	5.57	44.13	38.17	3.03	175.82	30.18	7.49	138.94	171.56	38.22	2.15	749.79	14.33	30.01	55.06	10.97	2.52	10.81	8.14	3.97	3.57	0.56	10.24	5.52	26.06	0.381	171.98
56L	747	B	19.73	1.34	8.34	3.58	2.90	0.106	2.98	0.21	0.08	0.90	6.09	42.83	37.69	2.92	174.84	30.42	6.91	145.50	171.79	39.53	1.47	755.87	14.68	30.28	56.65	11.31	2.63	11.29	8.39	4.05	3.49	0.57	10.41	5.32	24.50	0.438	146.70
55L	755	B	20.14	1.14	9.05	3.59	2.90	0.103	2.65	0.24	0.08	0.88	7.33	47.71	42.39	3.17	186.48	31.88	6.43	148.55	162.74	43.25	1.55	770.84	15.91	32.81	61.06	12.17	2.82	12.09	9.24	4.41	3.88	0.64	11.47	5.63	26.03	0.427	149.20
53L	771	B	20.43	1.25	9.88	3.46	3.29	0.124	2.58	0.22	0.14	0.85	6.69	47.69	45.60	3.00	187.74	32.06	10.12	143.36	151.80	43.49	2.64	746.21	16.32	33.36	62.15	12.37	2.90	12.31	9.44	4.41	3.67	0.62	11.69	5.54	27.13	0.452	187.01
52L	779	B	21.44	0.94	10.47	3.40	3.01	0.166	2.54	0.28	0.16	0.81	6.09	50.30	81.43	3.37	195.25	33.75	10.43	144.60	134.12	51.31	4.17	746.30	17.58	36.35	66.65	13.57	3.16	13.49	10.78	5.18	4.35	0.78	13.01	5.81	30.03	0.528	166.46
51L	787	B	20.94	1.22	8.29	3.66	3.20	0.093	2.78	0.20	0.14	0.92	5.37	50.95	44.67	3.03	190.30	32.37	7.85	150.82	159.19	44.48	2.93	737.96	16.34	33.21	62.06	12.48	2.89	12.23	9.44	4.59	3.98	0.63	11.98	5.90	28.49	0.500	178.26
49L	803	B	20.50	1.41	8.19	3.65	3.01	0.099	2.95	0.18	0.12	0.93	4.63	49.55	41.72	3.11	184.02	31.94	10.12	150.61	178.41	43.63	2.00	760.68	15.94	32.78	61.31	12.39	2.78	12.15	9.27	4.49	3.87	0.62	11.46	5.45	26.87	0.420	145.61
48L	811	B	18.73	1.39	6.84	3.46	2.68	0.076	3.33	0.17	0.07	0.90	4.29	37.50	34.71	3.07	161.79	28.92	5.21	143.61	180.34	35.81	1.67	715.67	13.30	27.57	51.20	10.26	2.39	10.19	7.64	3.73	3.15	0.52	9.48	4.32	24.83	0.390	128.74
46L	827	B	20.63	1.18	8.02	3.71	2.97	0.101	3.08	0.18	0.08	0.94	5.45	34.14	41.15	3.04	184.05	31.75	4.68	148.95	164.28	40.20	2.52	746.68	15.14	31.62	58.22	11.85	2.66	11.57	8.71	4.07	3.50	0.60	10.88	5.43	25.53	0.412	144.40
44L	846	B	20.05	1.45	9.87	3.59	2.81	0.159	2.84	0.21	0.06	0.88	5.45	39.42	40.66	3.13	174.46	30.51	6.00	147.41	173.89	38.80	2.02	736.51	14.71	30.44	55.55	11.27	2.57	10.86	8.24	4.02	3.44	0.59	10.64	5.05	27.07	0.479	132.73
42L	862	B	19.43	1.36	8.55	3.53	2.89	0.100	3.20	0.20	0.07	0.93	5.05	35.96	37.65	3.13	169.22	30.13	5.03	143.19	174.37	40.07	2.50	735.36	14.92	30.85	57.56	11.55	2.67	11.43	8.48	4.18	3.64	0.67	10.70	5.19	24.34	0.519	135.55
40L	878	B	20.01	1.25	8.61	3.69	2.95	0.088	3.02	0.18	0.06	0.93	6.57	26.84	41.37	3.17	180.73	31.22	7.19	148.71	173.55	41.89	2.85	768.52	15.33	31.58	58.50	11.71	2.68	11.55	8.76	4.25	3.80	0.62	10.96	5.17	26.08	0.417	136.56
38L	894	B	19.48	1.17	9.62	3.44	2.84	0.108	2.67	0.21	0.08	0.85	5.70	44.37	44.90	3.19	180.16	31.65	7.40	147.82	158.74	43.99	4.31	740.54	16.25	33.22	61.78	12.57	2.85	12.36	9.37	4.53	3.81	0.66	12.11	5.67	27.41	0.499	141.21
37L	904	B	18.53	1.34	8.84	3.40	2.87	0.086	1.96	0.19	0.07	0.87	4.43	70.71	40.42	3.40	170.03	30.93	8.02	151.41	182.37	46.51	0.96	762.80	15.47	32.12	58.56	11.72	2.82	11.92	9.37	4.78	4.34	0.59	11.24	4.80	23.76	0.381	141.81
36L	912	B	18.75	1.33	9.55	3.42	2.86	0.123	1.87	0.21	0.06	0.86	6.38	76.96	47.80	5.14	173.49	30.97	10.36	152.04	180.34	47.27	1.02	769.72	15.77	32.57	58.97	11.96	2.90	12.12	9.60	5.01	4.45	0.63	11.44	6.55	24.70	0.453	143.21
35L	920	B	18.45	1.22	8.08	3.36	2.82	0.079	1.90	0.19	0.04	0.88	7.11	45.14	41.62	4.47	176.48	31.06	7.05	151.53	176.87	46.23	0.70	743.66	15.69	32.48	59.69	11.99	2.88	12.08	9.49	4.78	4.28	0.57	11.42	5.25	23.61	0.411	141.69
33L	936	B	18.61	1.29	10.47	3.45	3.11	0.105	1.81	0.23	0.08	0.88	4.34	61.25	67.39	2.93	179.02	31.90	12.94	145.65	168.37	48.42	1.34	767.88	16.57	34.16	63.05	12.69	3.06	12.80	10.02	4.98	4.45	0.63	12.24	6.78	24.45	0.378	141.94
32L	944	B	19.98	1.17	10.07	3.55	2.88	0.133	1.59	0.22	0.08	0.83	5.18	96.61	72.58	5.92	183.76	33.13	8.16	157.01	176.84	49.09	1.40	760.64	17.02	35.43	62.82	12.62	2.99	12.79	10.02	5.14	4.65	0.64	12.70	6.68	29.29	0.488	146.32
31L	952	B	18.61	1.36	7.88	3.48	2.98	0.076	1.97	0.20	0.05	0.93	6.27	64.81	40.08	3.37	175.97	31.03	8.89	154.93	190.02	44.38	0.66	767.28	15.18	31.35	57.29	11.57	2.86	11.57	9.11	4.65	4.12	0.61	10.94	5.29	23.65	0.459	149.68
29L	969	B	19.21	1.38	9.41	3.55	3.03	0.108	1.84	0.23	0.08	0.90	5.01	47.64	65.83	2.60	182.17	31.65	11.55	151.78	175.95	46.75	0.97	781.94	16.16	33.05	61.02	12.35	2.98	12.36	9.69	4.86	4.19	0.59	11.85	4.82	26.13	0.431	144.59
27L	981	B	18.60	1.40	8.65	3.32	3.10	0.054	2.19	0.19	1.27	0.92	4.83	74.22	56.69	3.35	173.18	30.09	10.25	147.64	175.97	43.76	11.27	698.87	14.82	30.58	55.22	11.16	2.75	11.19	8.89	4.57	4.02	0.57	10.93	6.55	33.44	0.642	170.49
25L	996	B	19.04	1.17	8.38	3.56	3.04	0.087	1.84	0.21	0.04	0.88	4.70	54.66	48.40	4.22	174.61	31.74	8.65	154.64	182.34	44.94	0.59	770.79	15.30	32.22	58.63	11.85	2.90	12.09	9.29	4.66	4.01	0.57	11.35	5.46	23.12	0.401	143.71
24L	1003	B	18.84	1.36	8.31	3.47	3.00	0.084	1.88	0.20	0.07	0.90	5.18	57.29	41.53	1.87	174.39	30.66	10.17	152.87	185.31	45.21	0.95	761.08	15.30	31.30	57.76	11.77	2.82	11.58	9.25	4.69	4.21	0.59	11.14	4.96	23.81	0.452	147.91
22L	1017	B	19.39	1.21	8.72	3.60	3.13	0.090	1.96	0.21	0.05	0.86	6.46	59.50	49.27	2.66	174.20	31.72	8.16	153.98	182.71	44.80	0.75	773.59	15.60	32.03	59.56	12.02	2.91	12.05	9.35	4.70	4.09	0.57	11.49	5.41	23.02	0.390	148.29
20L	1033	B	19.82	1.18	9.57	3.67	3.27	0.116	1.74	0.22	0.07	0.88	7.10	78.84	69.74	2.16	187.92	33.30	8.97	155.30	177.95	49.28	1.41	751.27	16.18	33.37	61.26	12.53	3.02	12.42	10.04	5.18	4.59	0.67	12.08	5.60	25.56	0.479	155.87
18L	1049	B	19.81	1.17	9.85	3.66	3.51	0.100	1.69	0.20	0.06	0.85	6.28	75.42	71.30	3.53	193.52	33.09	10.38	156.81	169.11	50.24	1.84	741.69	16.08	33.47	61.38	12.51	3.11	12.76	10.27	5.34	4.73	0.71	12.23	5.71	25.55	0.519	164.88
16L	1065	B	19.97	1.53	10.19	3.62	4.04	0.109	1.61	0.22	0.07	0.85	6.57	61.06	76.32	3.37	196.32	32.97	8.78	155.26	169.27	49.27	1.77	701.10	16.06	33.23	60.22	12.39	3.06	12.41	10.08	5.09	4.54	0.65	12.16	4.95	26.66	0.410	208.53
14L	1081	A	18.35	2.35	10.47	2.98	4.39	0.056	1.86	0.85	2.65	0.58	7.56	82.59	87.12	3.72	188.22	29.37	8.15	144.18	239.42	44.70	6.92	504.49	14.67	30.76	54.76	11.18	2.76	11.42	9.44	4.88	4.34	0.62	11.95	5.75	57.56	0.786	284.51
13L	1089	A	17.53	4.41	10.27	2.88	3.63	0.046	2.18	0.23	4.85	0.67	3.69	78.69	83.00	2.75	163.96	27.84	10.18	204.89	508.25	45.15	7.24	543.20	14.77	30.70	54.36	11.15	2.72	11.32	9.28	4.76	4.19	0.61	11.47	5.96	56.69	0.946	230.22
12L	1098	A	16.22	5.32	10.82	2.78	3.64	0.063	2.03	0.29	6.83	0.69	7.22	79.82	75.63	3.09	166.14	26.28	7.49	228.85	598.57	43.55	13.54	539.37	13.67	28.91	50.85	10.34	2.56	10.68	8.73	4.57	4.15	0.58	10.69	6.21	89.02	1.737	227.84
11L	1120	A	17.15	5.79	9.40	2.97	3.43	0.073	1.81	0.26	2.89	0.74	7.91	59.20	72.73	4.35	168.18	27.78	8.28	205.76	494.36	43.52	5.86	605.24	14.35	29.58	53.09	10.85	2.64	11.05	8.71	4.53	3.97	0.56	10.97	4.94	46.77	0.866	202.19
10L	1128	A	18.06	2.85	10.41	3.09	3.27	0.057	2.13	0.21	4.72	0.76	7.60	62.00	80.58	4.07	178.49	29.71	7.52	161.81	265.62	46.74	8.29	557.13	15.16	31.33	56.92	11.58	2.81	11.62	9.58	4.88	4.26	0.63	11.82	6.31	67.20	1.330	191.56
9L	1135	A	18.09	2.75	11.90	3.00	3.30	0.497	1.93	0.48	2.92	0.72	7.77	81.75	81.32	2.40	184.87	30.32	10.57	169.40	278.20	52.05	5.18	528.23	15.68	32.55	57.76	11.86	2.91	12.22	10.19	5.48	4.93	0.68	12.07	6.54	56.01	0.953	161.29
7L	1150	A	19.39	1.44	11.15	3.13	3.21	0.111	1.79	0.27	2.81	0.75	8.13	81.67	87.85	3.21	187.96	31.68	9.99	122.23	162.10	47.84	4.73	538.51	15.49	32.50	59.60	12.11	2.93	12.42	10.23	5.22	4.59	0.67	12.14	5.35	55.00	1.125	168.15
5L	1166	A	18.65	1.65	12.93	3.05	3.54	0.280	1.89	0.34	2.27	0.72	8.62	71.79	90.13	3.93	188.89	30.93	13.68	149.74	181.49	55.77	3.71	543.00	16.32	34.68	61.42	12.72	3.09	12.97	11.08	5.90	5.41	0.77	12.47	5.86	45.15	0.793	166.27
3L	1182	A	18.83	2.14	11.56	3.05	3.23	0.200	1.82	0.49	1.07	0.69	9.80	72.72	89.19	5.01	181.41	30.80	11.27	136.99	195.35	50.16	4.36	552.62	15.80	32.83	59.82	12.31	2.96	12.45	10.35	5.33	4.72	0.72	12.07	5.17	35.81	0.562	144.00
2L	1190	A	18.80	2.18	10.97	3.17	3.41	0.054	2.04	0.22	4.39	0.76	8.50	69.65	87.88	3.32	183.33	30.89	10.13	142.54	157.51	49.75	10.11	525.19	15.85	32.91	59.63	12.12	2.98	12.49	10.12	5.11	4.53	0.64	12.50	6.12	86.31	2.090	197.50
1L	1198	A	18.01	2.53	12.15	2.96	4.28	0.262	2.31	0.51	1.59	0.68	9.20	66.17	86.75	2.11	187.83	29.35	8.75	152.85	210.66	48.47	6.22	486.16	15.30	31.32	56.83	11.56	2.81	11.81	9.59	4.94	4.39	0.66	12.08	5.18	38.83	0.796	234.86

Table S2

	Lab code	Unit	Depth (cm)	$^{206}Pb/^{204}Pb$	$^{207}Pb/^{204}Pb$	$^{208}Pb/^{204}Pb$	$^{207}Pb/^{206}Pb$	$^{208}Pb/^{206}Pb$	T_{mod} (Ma)	μ	κ
Leachate	129L	E	50	18.677	15.675	38.777	0.83930	2.07610	108.9	9.750	3.940
Leachate	128L	E	58	17.988	15.606	37.854	0.86760	2.10440	511.8	9.700	3.890
Leachate	127L	E	66	18.053	15.610	37.930	0.86470	2.10100	470.8	9.700	3.890
Leachate	126L	E	74	17.906	15.594	37.724	0.87090	2.10670	554.2	9.690	3.870
Leachate	125L	E	82	17.928	15.596	37.756	0.86990	2.10590	541.5	9.690	3.870
Leachate	124L	E	90	18.360	15.643	38.361	0.85200	2.08940	294.6	9.730	3.920
Leachate	123L	E	98	18.439	15.649	38.468	0.84870	2.08620	246.2	9.730	3.930
Leachate	122L	E	120	18.315	15.638	38.306	0.85390	2.09150	320.6	9.720	3.920
Leachate	121L	E	128	18.522	15.662	38.606	0.84560	2.08430	203.0	9.740	3.940
Leachate	120L	E	136	18.464	15.663	38.542	0.84830	2.08740	244.9	9.750	3.950
Leachate	119L	E	144	18.435	15.657	38.503	0.84930	2.08870	259.0	9.750	3.950
Leachate	118L	E	152	18.299	15.642	38.297	0.85480	2.09280	336.4	9.730	3.920
Leachate	117L	E	163	18.238	15.637	38.209	0.85740	2.09510	373.4	9.730	3.920
Leachate	116L	E	168	18.457	15.666	38.518	0.84880	2.08700	253.4	9.760	3.940
Leachate	115L	E	174	18.427	15.657	38.474	0.84970	2.08800	264.5	9.750	3.940
Leachate	114L	E	182	18.503	15.661	38.574	0.84640	2.08480	215.8	9.750	3.940
Leachate	113L	E	190	18.327	15.644	38.328	0.85360	2.09140	318.9	9.730	3.920
Leachate	112L	E	198	18.314	15.645	38.322	0.85430	2.09250	329.8	9.740	3.930
Leachate	111L	E	234	18.578	15.671	38.682	0.84350	2.08210	174.6	9.760	3.950
Leachate	110L	E	242	18.581	15.670	38.684	0.84340	2.08180	171.4	9.760	3.950
Leachate	109L	E	250	18.375	15.646	38.395	0.85150	2.08950	288.1	9.730	3.930
Leachate	108L	E	258	18.458	15.653	38.510	0.84800	2.08640	237.3	9.730	3.930
Leachate	107L	E	266	18.565	15.666	38.660	0.84380	2.08240	177.2	9.750	3.940
Leachate	106L	E	274	18.634	15.673	38.754	0.84110	2.07990	137.2	9.750	3.950
Leachate	105L	E	282	18.667	15.677	38.793	0.83980	2.07820	118.0	9.760	3.950
Leachate	104L	E	290	18.684	15.680	38.816	0.83920	2.07750	109.7	9.760	3.950
Leachate	103L	E	298	18.684	15.680	38.802	0.83920	2.07670	110.4	9.760	3.940
Leachate	102L	D	342	18.666	15.677	38.793	0.83980	2.07820	118.8	9.760	3.950
Leachate	101L	D	348	18.662	15.674	38.783	0.83990	2.07820	118.1	9.750	3.950
Leachate	100L	D	356	18.656	15.674	38.775	0.84020	2.07850	122.8	9.750	3.950
Leachate	99L	D	364	18.661	15.675	38.783	0.84000	2.07820	120.7	9.760	3.950
Leachate	98L	D	372	18.689	15.680	38.802	0.83890	2.07610	105.8	9.760	3.940
Leachate	97L	D	380	18.673	15.681	38.805	0.83980	2.07830	119.7	9.770	3.950
Leachate	96L	D	388	18.693	15.681	38.824	0.83880	2.07690	104.7	9.760	3.950
Leachate	95L	D	396	18.679	15.680	38.799	0.83940	2.07730	114.2	9.760	3.940
Leachate	94L	D	441	18.666	15.679	38.792	0.84000	2.07840	122.2	9.760	3.950
Leachate	93L	D	449	18.664	15.678	38.787	0.84000	2.07810	122.1	9.760	3.950
Leachate	92L	D	457	18.681	15.678	38.804	0.83920	2.07710	109.9	9.760	3.950
Leachate	91L	D	462	18.679	15.675	38.786	0.83920	2.07650	107.8	9.750	3.940
Leachate	90L	D	468	18.685	15.677	38.802	0.83900	2.07670	105.9	9.760	3.940
Leachate	89L	D	474	18.647	15.674	38.782	0.84060	2.07990	128.9	9.760	3.950
Leachate	88L	D	482	18.642	15.675	38.786	0.84088	2.08064	134.1	9.760	3.960
Leachate	87L	D	490	18.639	15.673	38.784	0.84090	2.08086	133.9	9.750	3.960
Leachate	86L	D	498	18.630	15.671	38.756	0.84113	2.08025	136.8	9.750	3.950
Leachate	85L	D	504	18.657	15.678	38.781	0.84033	2.07865	126.8	9.760	3.950
Leachate	84L	D	512	18.634	15.669	38.768	0.84087	2.08044	131.8	9.750	3.950
Leachate	83L	C	519	18.607	15.673	38.758	0.84233	2.08299	156.4	9.760	3.970
Leachate	82L	C	527	18.703	15.685	38.892	0.83861	2.07938	102.3	9.770	3.970
Leachate	81L	C	535	18.713	15.686	38.910	0.83821	2.07920	96.6	9.770	3.980
Leachate	80L	C	543	18.747	15.693	38.962	0.83708	2.07831	80.7	9.780	3.980
Leachate	79L	C	548	18.751	15.697	38.981	0.83714	2.07888	83.5	9.790	3.990
Leachate	78L	C	554	18.753	15.695	38.971	0.83688	2.07811	78.8	9.790	3.980
Leachate	ZL	C	562	18.760	15.696	38.990	0.83666	2.07828	75.2	9.790	3.990
Leachate	77L	C	570	18.762	15.697	38.994	0.83668	2.07844	76.5	9.790	3.990
Leachate	76L	C	578	18.759	15.696	38.989	0.83673	2.07853	76.4	9.790	3.990
Leachate	75L	C	590	18.744	15.693	38.969	0.83719	2.07904	82.5	9.780	3.980
Leachate	74L	C	597	18.754	15.695	38.982	0.83689	2.07868	78.5	9.790	3.990
Leachate	73L	C	613	18.735	15.691	38.947	0.83753	2.07884	87.4	9.780	3.980
Leachate	72L	C	621	18.714	15.685	38.896	0.83814	2.07843	94.9	9.770	3.970
Leachate	71L	C	627	18.733	15.689	38.919	0.83751	2.07763	86.3	9.780	3.970
Leachate	70L	C	633	18.707	15.683	38.883	0.83837	2.07851	97.8	9.770	3.970
Leachate	69L	C	641	18.744	15.688	38.962	0.83698	2.07867	77.4	9.770	3.980
Leachate	68L	C	649	18.756	15.685	38.919	0.83627	2.07504	64.9	9.770	3.960
Leachate	67L	B	657	18.740	15.693	38.949	0.83741	2.07842	85.8	9.780	3.980
Leachate	66L	B	664	18.744	15.684	38.918	0.83675	2.07636	72.2	9.770	3.960
Leachate	65L	B	670	18.780	15.691	38.945	0.83553	2.07372	55.6	9.780	3.950
Leachate	64L	B	678	18.756	15.698	38.970	0.83699	2.07775	81.9	9.790	3.980
Leachate	63L	B	686	18.743	15.689	38.960	0.83701	2.07854	78.7	9.770	3.980
Leachate	62L	B	692	18.748	15.694	38.961	0.83709	2.07814	81.4	9.780	3.980
Leachate	61L	B	707	18.729	15.691	38.935	0.83782	2.07885	92.0	9.780	3.980
Leachate	60L	B	715	18.752	15.695	38.974	0.83699	2.07836	80.1	9.790	3.980
Leachate	59L	B	723	18.746	15.694	38.961	0.83720	2.07831	83.6	9.790	3.980
Leachate	58L	B	731	18.738	15.690	38.951	0.83736	2.07871	84.4	9.780	3.980
Leachate	57L	B	739	18.735	15.693	38.953	0.83761	2.07915	89.4	9.780	3.980
Leachate	56L	B	747	18.748	15.691	38.962	0.83694	2.07815	78.3	9.780	3.980
Leachate	55L	B	755	18.745	15.690	38.954	0.83710	2.07810	79.8	9.780	3.980
Leachate	53L	B	771	18.759	15.689	38.961	0.83630	2.07690	67.8	9.770	3.970
Leachate	52L	B	779	18.730	15.691	38.940	0.83770	2.07900	91.5	9.780	3.980
Leachate	51L	B	787	18.754	15.692	38.961	0.83670	2.07740	75.9	9.780	3.980
Leachate	49L	B	803	18.728	15.690	38.931	0.83777	2.07870	90.7	9.780	3.980
Leachate	48L	B	811	18.718	15.688	38.920	0.83810	2.07930	95.5	9.780	3.980
Leachate	46L	B	827	18.764	15.696	38.982	0.83650	2.07750	72.8	9.790	3.980
Leachate	44L	B	846	18.753	15.697	38.986	0.83700	2.07880	82.0	9.790	3.990
Leachate	42L	B	862	18.754	15.696	38.990	0.83690	2.07890	79.5	9.790	3.990
Leachate	40L	B	878	18.757	15.697	38.984	0.83690	2.07840	79.2	9.790	3.980
Leachate	38L	B	894	18.741	15.691	38.960	0.83720	2.07880	82.7	9.780	3.980
Leachate	37L	B	904	18.701	15.690	38.899	0.83900	2.08020	109.9	9.780	3.980
Leachate	36L	B	912	18.725	15.691	38.942	0.83800	2.07980	94.3	9.780	3.980
Leachate	35L	B	920	18.754	15.696	38.979	0.83690	2.07850	79.9	9.790	3.980
Leachate	33L	B	936	18.721	15.691	38.939	0.83820	2.07990	98.0	9.780	3.980
Leachate	32L	B	944	18.718	15.690	38.946	0.83820	2.08060	98.1	9.780	3.990
Leachate	31L	B	952	18.734	15.690	38.941	0.83750	2.07880	86.6	9.780	3.980
Leachate	29L	B	969	18.754	15.692	38.959	0.83670	2.07740	75.4	9.780	3.980
Leachate	27L	B	981	18.742	15.687	38.932	0.83700	2.07730	77.9	9.770	3.970
Leachate	25L	B	996	18.736	15.694	38.957	0.83760	2.07920	90.4	9.790	3.980
Leachate	24L	B	1003	18.739	15.689	38.946	0.83730	2.07840	82.7	9.780	3.980
Leachate	22L	B	1017	18.752	15.691	38.970	0.83670	2.07820	75.1	9.780	3.980
Leachate	20L	B	1033	18.747	15.692	38.967	0.83700	2.07850	79.5	9.780	3.980
Leachate	18L	B	1049	18.756	15.694	38.979	0.83670	2.07830	76.2	9.780	3.980
Leachate	16L	B	1065	18.735	15.693	38.952	0.83760	2.07910	89.5	9.780	3.980
Leachate	14L	A	1081	18.737	15.685	38.916	0.83710	2.07690	79.1	9.770	3.960
Leachate	13L	A	1089	18.737	15.686	38.915	0.83720	2.07690	79.8	9.770	3.960
Leachate	12L	A	1098	18.720	15.678	38.873	0.83750	2.07660	82.6	9.760	3.950
Leachate	11L	A	1120	18.723	15.685	38.902	0.83770	2.07770	88.1	9.770	3.970
Leachate	10L	A	1128	18.735	15.685	38.912	0.83720	2.07690	79.1	9.770	3.960
Leachate	9L	A	1135	18.729	15.686	38.911	0.83750	2.07760	85.1	9.770	3.970
Leachate	7L	A	1150	18.741	15.687	38.930	0.83700	2.07720	77.5	9.770	3.970
Leachate	5L	A	1166	18.748	15.688	38.938	0.83680	2.07700	74.6	9.770	3.970
Leachate	3L	A	1182	18.738	15.687	38.931	0.83720	2.07770	80.7	9.770	3.970
Leachate	2L	A	1190	18.747	15.686	38.917	0.83670	2.07600	72.6	9.770	3.960
Leachate	1L	A	1198	18.734	15.686	38.919	0.83730	2.07740	82.3	9.770	3.970
Residue	104 R	E	290	18.760	15.691	38.959	0.83650	2.07680	70.0	9.778	3.971
Residue	101 R	D	348	18.753	15.691	38.948	0.83670	2.07680	74.8	9.779	3.970
Residue	98 R	D	372	18.774	15.698	38.973	0.83610	2.07580	67.7	9.789	3.971
Residue	94 R	D	441	18.733	15.684	38.892	0.83730	2.07620	80.8	9.767	3.956
Residue	91 R	D	462	18.722	15.681	38.871	0.83760	2.07620	84.1	9.761	3.952
Residue	89 R	D	474	18.724	15.681	38.881	0.83750	2.07660	83.3	9.762	3.956
Residue	77 R	C	570	18.742	15.689	38.973	0.83710	2.07950	80.4	9.776	3.987
Residue	69 R	C	641	18.728	15.688	38.909	0.83760	2.07770	88.5	9.775	3.967
Residue	61 R	B	707	18.744	15.695	38.987	0.83740	2.08010	85.7	9.787	3.993
Residue	52 R	B	779	18.793	15.699	39.000	0.83530	2.07520	55.8	9.790	3.972
Residue	43 R	B	851.5	18.748	15.693	38.985	0.83710	2.07950	81.1	9.783	3.989
Residue	35 R	B	920	18.736	15.694	38.986	0.83760	2.08070	90.6	9.786	3.996
Residue	26 R	B	988.5	18.738	15.696	38.968	0.83770	2.07960	91.4	9.789	3.988
Residue	17 R	B	1057	18.776	15.694	38.993	0.83590	2.07670	61.8	9.782	3.977
Residue	10 R	A	1128	18.787	15.698	39.025	0.83550	2.07710	58.1	9.788	3.986

Depth (cm)	Laboratory code	Material	$\delta^{13}C$	^{14}C age (BP)	Calendar age (BC-AD) (2 σ)
186	Lyon-9957 (SacA 32583)	Vegetal matter	-26.6	665 ± 30	1276 -1391 AD
362	Lyon-9959 (SacA 32584)	Wood	-30.8	1455 ± 30	558 - 649 AD
460	Lyon-9960 (SacA 32585)	Seeds	-31.3	2020 ± 30	106 BC - 58 AD
680-690	UGAMS (17652)	Pollen	-27.8	2000 ± 40	111 BC - 83 AD
1080-1090	UGAMS (17352)	Seeds	-25.9	1990 ± 25	43 BC - 63 AD
1189	Lyon-9962 (SacA 32587)	Vegetal matter	-31.9	2040 ± 30	163 BC - 47 AD

Table S3